Effects of Coulomb collisions on lower hybrid drift waves inside a laboratory reconnection current sheet

Cite as: Phys. Plasmas **29**, 022109 (2022); doi: 10.1063/5.0052555
Submitted: 31 March 2021 · Accepted: 23 January 2022 ·
Published Online: 16 February 2022

View Online Export Citation CrossMark

Jongsoo Yoo,[1,a)] Yibo Hu,[2] Jeong-Young Ji,[3] Hantao Ji,[1,4] Masaaki Yamada,[1] Aaron Goodman,[1] Kendra Bergstedt,[1] William Fox,[1] and Andrew Alt[1]

AFFILIATIONS

[1]Princeton Plasma Physics Laboratory, Princeton, New Jersey 08543, USA
[2]School of Physical Science and Technology, Soochow University, Suzhou 215006, China
[3]Department of Physics, Utah State University, Logan, Utah 84322, USA
[4]Department of Astrophysical Sciences, Princeton University, Princeton, New Jersey 08544, USA

Note: This paper is part of the Special Collection: Frontiers of Magnetic Reconnection Research in Heliophysical, Astrophysical and Laboratory Plasmas.
[a)]**Author to whom correspondence should be addressed:** jyoo@pppl.gov

ABSTRACT

We have developed a local, linear theoretical model for lower hybrid drift waves that can be used for plasmas in the weakly collisional regime. Two cases with typical plasma and field parameters for the current sheet of the magnetic reconnection experiment have been studied. For a case with a low electron beta ($\beta_e = 0.25$, high guide field case), the quasi-electrostatic lower hybrid drift wave is unstable, while the electromagnetic lower hybrid drift wave has a positive growth rate for a high-β_e case ($\beta_e = 8.9$, low guide field case). For both cases, including the effects of Coulomb collisions reduces the growth rate but collisional impacts on the dispersion and growth rate are limited ($\lesssim$20%).

I. INTRODUCTION

Magnetic reconnection converts magnetic energy into plasma thermal and flow energy via topological rearrangements of the magnetic field lines. Energy conversion processes during magnetic reconnection result in many free energy sources for waves and instabilities near the diffusion region, such as strong gradients of the magnetic field and plasma parameters. Among them, the lower hybrid drift wave (LHDW) has been widely observed near the diffusion region in both space (e.g., Refs. 1–7) and laboratory plasmas (e.g., Refs. 8–10). The free energy source of LHDWs is the cross field current.[11] The large density gradients near the separatrix can particularly be a free energy source by inducing a perpendicular current via a diamagnetic drift.

LHDWs have been a candidate for generating anomalous resistivity because it can interact differently with magnetized electrons and non-magnetized ions, resulting in momentum exchange between the two species (e.g., Refs. 7–9 and 12–16). For reconnection with a negligible guide field, the fast-growing, short-wavelength ($k\rho_e \sim 1$; k is the magnitude of the wave vector $\mathbf{k}$, ρ_e is the electron gyroradius), quasi-electrostatic LHDW (ES-LHDW) is found to be localized at the edge of the current sheet[8] due to the stabilization by the high plasma beta (β).[17] On the other hand, the long-wavelength ($k\sqrt{\rho_e\rho_i} \sim 1$; ρ_i is the ion gyroradius), electromagnetic LHDW (EM-LHDW) that propagates obliquely to the magnetic field exists in the electron diffusion region.[9] However, extensive efforts via numerical particle-in-cell (PIC) simulations[15,16] show that the EM-LHDW does not play an important role in fast reconnection and electron energization near the electron diffusion region during antiparallel reconnection.

Recent observations by the magnetospheric multiscale (MMS) mission show that the ES-LHDW can be generated inside or near the electron diffusion region,[5–7] when there is a sizable guide field. The ES-LHDW can drive electron heating and vortical flows[6] near the electron diffusion region. Moreover, the ES-LHDW is capable of generating anomalous drag between electrons and ions.[7]

Motivated by these observations, Yoo *et al.*[7] have developed a local, linear theoretical model that explains the dynamics of both ES- and EM-LHDWs in the presence of a guide field. This model is based on collisionless closures for the electron heat flux with the assumption of a gyrotropic electron pressure tensor. The results from the model agree with the activities of the ES- and EM-LHDWs inside a current sheet at the magnetopause.[7]

In laboratory experiments, such as the magnetic reconnection experiment (MRX), the effects of Coulomb collisions on magnetic reconnection and electron heating are not negligible. The classical Spitzer resistivity,[18] for example, can balance the reconnection electric field in the collisional regime and can even account for 10%–20% of that in the collisionless regime.[19,20] This indicates that Coulomb collisions may also affect the dynamics of LHDWs in laboratory plasmas.

These collisional effects on LHDWs have not been considered previously, even though LHDWs in the reconnection current sheet have been extensively studied via theoretical analyses and numerical simulations (e.g., Refs. 11, 14, 21–23). This paper provides the first quantitative study of the effects of Coulomb collisions on LHDWs. Through this model, we can address how the dynamics of LHDWs in laboratory plasmas are different from those in collisionless plasmas and when collisional effects become important. To include the effects from collisions, we have advanced the previous models[7,24] by using closures of the electron heat flux, heat generated by collisions, and resistivity that can be used for plasmas with arbitrary collisionality.[25,26] For a self-consistent modeling of the heat flux and energy conservation, we also have allowed a first-order perturbation of the perpendicular electron temperature ($T_{e1}^{\perp}$), which was set to be zero in a previous model by Yoo *et al.*[7] Unlike previous models, the zeroth-order electron temperature anisotropy is not allowed in the current model because the available closures were developed under the assumption of isotropic electron pressure at equilibrium. Except these changes, all other assumptions are the same: we used a kinetic equation for unmagnetized ions, fluid equations for electrons, and a gyrotropic pressure tensor for electrons.

This linear model can be used to quantify the effects of LHDWs on electron heating and reconnection dynamics in weakly collisional plasmas; with measured wave amplitudes and quasi-linear arguments, wave-associated anomalous terms and heat generated by collisions with ions can be directly estimated. It should be noted that the wave-associated heating power cannot be estimated by collisionless models.

In Sec. II, we explain the theoretical model for LHDWs in a local geometry. Then, in Sec. III, we numerically calculate dispersion relations of LHDWs for two cases. The biggest difference in the two cases is the value of electron beta, β_e. For the low-β_e case, which represents conditions near the electron diffusion region during reconnection with a strong guide field, the ES-LHDW is unstable. For the high-β_e case, which represents conditions in the same region but with a negligible guide field, the EM-LHDW has positive growth rates. In both cases, collisional effects on LHDWs with typical MRX parameters are not significant ($\lesssim$20 %). Finally, in Sec. IV, we discuss the results and propose future research.

II. DERIVATION OF THE DISPERSION RELATION

Figure 1 shows the geometry of our local theoretical model for a LHDW inside a current sheet. Here, the subscript 0 indicates equilibrium quantities. We chose the ion rest frame, and electrons have velocity ($\mathbf{u}_{e0}$) on the x–z plane. The equilibrium magnetic field is along the z direction and the density gradient direction is along the y direction. In this model, there is neither equilibrium temperature gradient nor

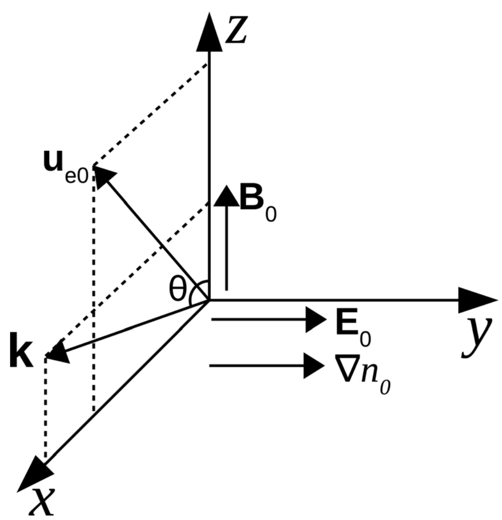

FIG. 1. Geometry of the local theory for the LHDW dispersion calculation. We are working in the ion rest frame with the z direction toward the equilibrium magnetic field ($\mathbf{B}_0$) and the y direction along the density gradient direction. Due to the force balance, the equilibrium electric field $\mathbf{E}_0$ is also along the y direction. The equilibrium electron flow velocity $\mathbf{u}_{e0}$ and wave vector $\mathbf{k}$ reside on the x–z plane. The angle between $\mathbf{k}$ and $\mathbf{B}_0$ is given by θ.

ion temperature anisotropy. The equilibrium electron temperature is also assumed to be isotropic, but anisotropy is allowed in the perturbed electron temperature. The wave vector ($\mathbf{k}$) lies on the x–z plane due to our assumption of negligible k_y. Thus, our theoretical model is local and valid only when the wavelength of the LHDW is much smaller than the thickness of the current sheet in the y direction.[24]

To balance the force associated with the pressure (density) gradient, there is an equilibrium electric field along the y direction. By using the ion and electron force balance equations, the equilibrium electric field E_0 can be expressed in terms of other plasma parameters. From the ion force balance along the y direction, we have

$$en_0 E_0 = T_{i0}\frac{dn_0}{dy} = \varepsilon n_0 T_{i0}, \tag{1}$$

where n_0 is the equilibrium density, T_{i0} is the equilibrium ion temperature, and $\varepsilon = (dn_0/dy)/n_0$ is the inverse of the density gradient scale. From the y component of the electron momentum equation, we have

$$-en_0(E_0 - u_{e0x}B_0) = T_{e0}\frac{dn_0}{dy}, \tag{2}$$

where u_{e0x} is the x component of the equilibrium electron flow velocity and T_{e0} is the equilibrium electron temperature. Then, the equilibrium electric field is

$$E_0 = \frac{T_{i0}}{T_{e0}+T_{i0}} u_{e0x}B_0. \tag{3}$$

The inverse of the gradient scale is given by

$$\varepsilon = \frac{eu_{e0x}B_0}{T_{e0}+T_{i0}}. \tag{4}$$

Note that Eqs. (3) and (4) are the same as those in the collisionless model in Yoo *et al.*,[7] because the resistivity term is zero along the y direction.

All perturbed quantities have a normal mode decomposition proportional to $\exp[i(\mathbf{k}\cdot\mathbf{x}-\omega t)]$ with the wave vector $\mathbf{k}=(k_\perp,0,k_\parallel)$. Here, the subscript 1 indicates perturbed quantities. For the dispersion relation, Maxwell's equations without the displacement current term are used,

$$\mathbf{k}\times(\mathbf{k}\times\mathbf{E}_1)=-i\omega\mu_0\mathbf{J}_1. \tag{5}$$

The displacement current term is ignored because the phase velocity of the wave is much smaller than the speed of light.

Assuming the equilibrium ion distribution function to be locally Maxwellian, the perturbed ion current density ($\mathbf{J}_{i1}$) is given by[24]

$$\mathbf{J}_{i1}=-\frac{in_0e^2}{m_ikv_{ti}}\left[Z(\zeta)\mathbf{E}_1+\frac{Z''(\mathbf{E}_1\cdot\hat{\mathbf{k}})}{2}\hat{\mathbf{k}}-i\left(\frac{\varepsilon}{2k}\right)Z''E_{1y}\hat{\mathbf{k}}\right], \tag{6}$$

where m_i is the ion mass, $v_{ti}=\sqrt{2T_{i0}/m_i}$ is the ion thermal speed, $\zeta=\omega/kv_{ti}$, and $Z(\zeta)$ is the plasma dispersion function. This is from a perturbed Vlasov equation for unmagnetized ions. This means that any dynamics slower than the ion cyclotron frequency have been ignored, including collisional effects on ion dynamics. In our regime of interest, the ion collision frequency is smaller than the ion cyclotron frequency. The perturbed ion temperature can be also obtained, which is

$$T_{i1}=\frac{ie}{k}\left[\mathbf{E}_1\cdot\hat{\mathbf{k}}\left(2Z'+\frac{Z'''}{4}\right)-iE_{1y}\left(\frac{\varepsilon}{k}\right)\left(Z'+\frac{Z'''}{4}\right)\right]. \tag{7}$$

The perturbed electron current density $\mathbf{J}_{e1}$ is obtained from fluid equations. This is different from the classical formulation of LHDWs, where the kinetic (Vlasov) equation is used for electron dynamics (e.g., Refs. 17, 27, and 28). Since electrons are magnetized, a gyrotropic electron pressure tensor is assumed. In this case, the 3 + 1 fluid model (n, $\mathbf{u}$, $p^\parallel$, and $p^\perp$; $p^\parallel$ and $p^\perp$ are the parallel and perpendicular pressure, respectively) is appropriate.[25] In this fluid model, off diagonal terms of the electron pressure tensor are ignored.

The first-order electron momentum equation is given by

$$\begin{aligned}im_en_0(\omega-\mathbf{k}\cdot\mathbf{u}_{e0})\mathbf{u}_{e1}&=i\mathbf{k}\cdot\mathbf{P}_{e1}+en_0(\mathbf{E}_1+\mathbf{u}_{e1}\times\mathbf{B}_0+\mathbf{u}_{e0}\times\mathbf{B}_1)\\&\quad+e(\mathbf{E}_0+\mathbf{u}_{e0}\times\mathbf{B}_0)n_{e1}-\mathbf{R}_{e1},\end{aligned} \tag{8}$$

where $\mathbf{P}_{e1}$ is the perturbed electron pressure tensor and $\mathbf{R}_{e1}$ is the perturbed resistivity. The perturbed electron density n_{e1} is given by the electron continuity equation, which is

$$(\omega-\mathbf{k}\cdot\mathbf{u}_{e0})n_{e1}=(\mathbf{k}\cdot\mathbf{u}_{e1}-i\varepsilon u_{e1y})n_0. \tag{9}$$

To close the momentum equation, we need closures for $\mathbf{P}_{e1}$ and $\mathbf{R}_{e1}$. For $\mathbf{P}_{e1}$, we only need closures for $p_{e1}^\perp$ and $p_{e1}^\parallel$, since we assume a gyrotropic pressure tensor as mentioned earlier. To obtain $p_{e1}^\perp$ and $p_{e1}^\parallel$, we start from the following kinetic equation:

$$\frac{\partial f_e}{\partial t}+\mathbf{v}\cdot\nabla f_e-\frac{e}{m_e}(\mathbf{E}+\mathbf{v}\times\mathbf{B})\cdot\frac{\partial f_e}{\partial\mathbf{v}}=C(f_e), \tag{10}$$

where f_e is the electron distribution function and $C(f_e)$ is the collision operator. First, multiplying the kinetic equation with $m_e(v_z-u_{ez})^2$ and integrating over the velocity space yield

$$\frac{\partial p_e^\parallel}{\partial t}+\nabla\cdot(\mathbf{u}_ep_e^\parallel)+\nabla\cdot\mathbf{q}_e^\parallel+2\frac{\partial u_{ez}}{\partial z}p_e^\parallel=C_e^\parallel, \tag{11}$$

where

$$p_e^\parallel=m_e\int(v_z-u_{ez})^2f_ed\mathbf{v}, \tag{12}$$

$$\mathbf{q}_e^\parallel=m_e\int(\mathbf{v}-\mathbf{u}_e)(v_z-u_{ez})^2f_ed\mathbf{v}, \tag{13}$$

$$C_e^\parallel=\int C(f_e)m_e(\mathbf{v}-\mathbf{u}_e)^2d\mathbf{v}. \tag{14}$$

Similarly, multiplying the kinetic equation with $m_e[(v_x-u_{ex})^2+(v_y-u_{ey})^2]/2$ and integrating over the velocity space yield

$$\frac{\partial p_e^\perp}{\partial t}+\nabla\cdot(\mathbf{u}_ep_e^\perp)+\nabla\cdot\mathbf{q}_e^\perp+\left(\frac{\partial u_{ex}}{\partial x}+\frac{\partial u_{ey}}{\partial y}\right)p_e^\perp=C_e^\perp, \tag{15}$$

where

$$p_e^\perp=m_e\int\frac{1}{2}\left[(v_x-u_{ex})^2+(v_y-u_{ey})^2\right]f_ed\mathbf{v}, \tag{16}$$

$$\mathbf{q}_e^\perp=m_e\int\frac{1}{2}\left[(v_x-u_{ex})^2+(v_y-u_{ey})^2\right](\mathbf{v}-\mathbf{u}_e)f_ed\mathbf{v}, \tag{17}$$

$$C_e^\perp=\int\frac{1}{2}C(f_e)\left[(v_x-u_{ex})^2+(v_y-u_{ey})^2\right]d\mathbf{v}. \tag{18}$$

Linearizing Eq. (11) yields

$$\begin{aligned}&-i\omega p_{e1}^\parallel+\varepsilon u_{e1y}n_0T_{e0}+i(\mathbf{k}\cdot\mathbf{u}_0)p_{e1}^\parallel+i(\mathbf{k}\cdot\mathbf{u}_{e1})n_0T_{e0}\\&\quad+i\mathbf{k}\cdot\mathbf{q}_{e1}^\parallel+2ik_\parallel u_{e1z}n_0T_{e0}=C_{e1}^\parallel.\end{aligned} \tag{19}$$

By using $p_{e1}^\parallel=n_{e1}T_{e0}+n_0T_{e1}^\parallel$ and Eq. (9), Eq. (19) can be written as

$$i(\omega-\mathbf{k}\cdot\mathbf{u}_0)n_0T_{e1}^\parallel=i\mathbf{k}\cdot\mathbf{q}_{e1}^\parallel+2ik_\parallel u_{e1z}n_0T_{e0}-C_{e1}^\parallel. \tag{20}$$

Similarly, linearizing Eq. (15) yields

$$i(\omega-\mathbf{k}\cdot\mathbf{u}_0)n_0T_{e1}^\perp=i\mathbf{k}\cdot\mathbf{q}_{e1}^\perp+ik_\perp u_{e1x}n_0T_{e0}-C_{e1}^\perp. \tag{21}$$

We now need fluid closures for $\mathbf{q}_{e1}^\parallel$, $\mathbf{q}_{e1}^\perp$, $C_{e1}^\parallel$, and $C_{e1}^\perp$. First, the 3 + 1 fluid model gives us[7]

$$\mathbf{q}_e^\parallel=\frac{\hat{z}}{m_e\omega_{ce}}\times\left(p_e^\parallel\nabla T_e+T_e\nabla p_e^\parallel-\frac{T_e}{2}\nabla\pi_e^\parallel-T_e^\parallel\nabla p_e^\perp\right)+q_{ez}^\parallel\hat{z}, \tag{22}$$

where $\omega_{ce}=eB_0/m_e$, $\pi_e^\parallel=2(p_e^\parallel-p_e^\perp)/3$ and $T_e^\parallel=p_e^\parallel/n_e$. After linearization, the x component of $\mathbf{q}_{e1}^\parallel$ is

$$q_{e1x}^\parallel=\frac{2T_{e0}}{3(T_{e0}+T_{i0})}n_0u_{e0x}(T_{e1}^\parallel-T_{e1}^\perp)=r_{te}n_0u_{e0x}(T_{e1}^\parallel-T_{e1}^\perp), \tag{23}$$

where $r_{te}=2T_{e0}/3(T_{e0}+T_{i0})$. For $\mathbf{q}_e^\perp$, we derive a closure in Appendix A, which can be written as

$$\begin{aligned}\mathbf{q}_e^\perp=\frac{\hat{z}}{m_e\omega_{ce}}\times&\left[\left(-\frac{5}{6}p_e^\parallel+\frac{17}{6}p_e^\perp\right)\nabla T_e\right.\\&\left.-\left(\frac{2}{9}T_e^\parallel+\frac{4}{9}T_e^\perp\right)\nabla p_e^\parallel+\left(\frac{8}{9}T_e^\parallel-\frac{2}{9}T_e^\perp\right)\nabla p_e^\perp\right]+q_{ez}^\perp\hat{z}.\end{aligned} \tag{24}$$

After linearization, the x component of $\mathbf{q}_{e1}^\perp$ is

$$q_{e1x}^\perp=-\frac{2T_{e0}}{3(T_{e0}+T_{i0})}n_0u_{e0x}(T_{e1}^\parallel-T_{e1}^\perp)=-r_{te}n_0u_{e0x}(T_{e1}^\parallel-T_{e1}^\perp). \tag{25}$$

For $q_{e1z}^{\parallel}$ and $q_{e1z}^{\perp}$, we employ a closure for plasmas with arbitrary collisionality, which can be written as[25]

$$q_{e1z}^{\parallel} = \frac{6}{5} h_{e1}^{\parallel} + \sigma_{e1}^{\parallel}, \tag{26}$$

$$q_{e1z}^{\perp} = \frac{2}{5} h_{e1}^{\parallel} - \frac{1}{2} \sigma_{e1}^{\parallel}, \tag{27}$$

where

$$h_{e1}^{\parallel} = -\frac{1}{2} i\bar{k}_{\|}\bar{K}_{hh} n_0 v_{te} T_{e1}^{*} + i\bar{k}_{\|}\bar{K}_{h\sigma} v_{te}\pi_{e1}^{\parallel} + \bar{K}_{hR} n_0 T_{e0}(u_{e1z} - u_{i1z}) + i\bar{K}_{hS} v_{te}\pi_{e1}^{\parallel}, \tag{28}$$

$$\sigma_{e1}^{\parallel} = \frac{4}{3} i\bar{k}_{\|}\bar{K}_{h\sigma} n_0 v_{te} T_{e1}^{*} - i\bar{k}_{\|}\bar{K}_{\sigma\sigma} v_{te}\pi_{e1}^{\parallel} + \bar{K}_{\sigma R} n_0 T_{e0}(u_{e1z} - u_{i1z}) + i\bar{K}_{\sigma S} v_{te}\pi_{e1}^{\parallel}. \tag{29}$$

Here, $T_{e1}^{*} = T_{e1} + 2\pi_{e1}^{\parallel}/5n_0$, $v_{te} = \sqrt{2T_{e0}/m_e}$ is the electron thermal speed, and $\bar{k}_{\|} = k_{\|}\lambda_c$ is the normalized parallel wave number. The electron collision length is defined as $\lambda_c \equiv v_{te}\tau_{ee}$, and the electron–electron collision time τ_{ee} is given by

$$\tau_{ee} = \frac{6\sqrt{2}\pi^{3/2}\varepsilon_0^2\sqrt{m_e}T_{e0}^{3/2}}{n_0 e^4 \ln\Lambda_{ee}}, \tag{30}$$

where $\ln\Lambda_{ee}$ is the Coulomb logarithm for electron–electron collisions and ε_0 is the permittivity of free space. In Eqs. (28) and (29), $\bar{K}_{AB}$ represents a kernel function that is obtained from a 6400 moment solution.[25] The kernel function $\bar{K}_{AB}$ has the following form:

$$\bar{K}_{AB} = \frac{a\bar{k}_{\|}^{\alpha}}{1 + d_1\bar{k}_{\|}^{\delta} + d_2\bar{k}_{\|}^{2\delta} + d_3\bar{k}_{\|}^{3\delta} + d_4\bar{k}_{\|}^{4\delta} + d_5\bar{k}_{\|}^{5\delta} + d_6\bar{k}_{\|}^{6\delta}}, \tag{31}$$

where the values of coefficients, such as a, α, and δ in Eq. (31), are given in Table I in Ji and Joseph.[25] For a negative $\bar{k}_{\|}$, $\bar{K}_{AB}(\bar{k}_{\|}) = \bar{K}_{AB}(-\bar{k}_{\|})$ if $\alpha = 0$ or $\alpha = 2$. When $\alpha = 1$, $\bar{K}_{AB}(\bar{k}_{\|}) = -\bar{K}_{AB}(-\bar{k}_{\|})$. These closures are consistent with those of Hammett and Perkins[29] in the collisionless limit, and they become consistent with those of Braginskii[30] in the collisional limit.

The heat generated by the collision terms $C_{e1}^{\parallel}$ and $C_{e1}^{\perp}$ also needs a closure and can be written as

$$C_{e1}^{\parallel} = \frac{2}{3} Q_{e1} + S_{e1}^{\parallel}, \tag{32}$$

$$C_{e1}^{\perp} = \frac{2}{3} Q_{e1} - \frac{1}{2} S_{e1}^{\parallel}, \tag{33}$$

where Q_e is the heat generated by collisions and $S_e^{\parallel}$ is related to the temperature anisotropy.[25] The closure for $S_{e1}^{\parallel}$ is given by[25]

$$S_{e1}^{\parallel} = \frac{4}{3}\bar{k}_{\|}\bar{K}_{hS}\frac{n_0}{\tau_{ee}}T_{e1}^{*} + \frac{\bar{k}_{\|}}{\tau_{ee}}\bar{K}_{\sigma S}\pi_{e1}^{\parallel} + i\frac{8}{3}\bar{K}_{RS}\frac{n_0 T_{e0}}{v_{te}\tau_{ee}} \times (u_{e1z} - u_{i1z}) - \frac{2.05 - \bar{K}_{SS}}{\tau_{ee}}\pi_{e1}^{\parallel}. \tag{34}$$

The heat generated by collisions can be written as[26]

$$Q_e = 3\frac{m_e n_e}{m_i \tau_{ei}}(T_i - T_e) - \mathbf{u}_{ei}\cdot\mathbf{R}_e, \tag{35}$$

where τ_{ei} is the electron–ion collision time and $\mathbf{u}_{ei} = \mathbf{u}_e - \mathbf{u}_i$ is the relative flow velocity between electrons and ions. Assuming the ion charge status Z_i is unity, τ_{ei} is

$$\tau_{ei} = \frac{6\sqrt{2}\pi^{3/2}\varepsilon_0^2\sqrt{m_e}T_{e0}^{3/2}}{n_0 e^4 \ln\Lambda_{ei}}, \tag{36}$$

where $\ln\Lambda_{ei}$ is the Coulomb logarithm for electron–ion collisions. Linearizing Q_e yields

$$Q_{e1} = 3\frac{m_e n_{e1}}{m_i \tau_{ei}}(T_{i0} - T_{e0}) + 3\frac{m_e n_0}{m_i \tau_{ei}}(T_{i1} - T_{e1}) - \mathbf{u}_{e0}\cdot\mathbf{R}_{e1} - \mathbf{u}_{ei1}\cdot\mathbf{R}_{e0}. \tag{37}$$

We also need an expression for the resistivity. Since there is no temperature gradient in the equilibrium quantities, the zeroth-order resistivity $\mathbf{R}_{e0}$ can be written as[26]

$$\mathbf{R}_{e0} = -\alpha^{\|}\frac{m_e n_0}{\tau_{ei}}u_{e0z}\hat{\mathbf{z}} - \alpha^{\perp}\frac{m_e n_0}{\tau_{ei}}u_{e0x}\hat{\mathbf{x}}. \tag{38}$$

For $Z_i = 1$, the two coefficients are[26]

$$\alpha^{\|} = 0.504, \tag{39}$$

$$\alpha^{\perp} = 1 - \frac{1.46r + 1.06}{r^{\frac{5}{3}} - 0.081r^{\frac{4}{3}} + 2.97r + 2.13}, \tag{40}$$

where $r = \omega_{ce}\tau_{ee}$. There are additional terms in $\mathbf{R}_{e1}$ since temperature gradients exist in the first order. The parallel (z) component of $\mathbf{R}_{e1}$ is[25]

$$R_{e1}^{\|} = -i\frac{\bar{k}_{\|}\bar{K}_{hR}}{v_{te}\tau_{ee}}n_0 T_{e1}^{*} - i\frac{3}{4}\frac{\bar{k}_{\|}\bar{K}_{\sigma R}}{v_{te}\tau_{ee}}\pi_{e1}^{\|} - (1 - \bar{K}_{RR}) \times \frac{n_0 m_e}{\tau_{ee}}u_{ei1z} + i\frac{2\bar{K}_{RS}}{v_{te}\tau_{ee}}\pi_{e1}^{\|}. \tag{41}$$

Equation (41) can be written as

$$R_{e1}^{\|} = -ik_{\|}n_0\gamma_{ez}^{\|}T_{e1}^{\|} - ik_{\|}n_0\gamma_{ez}^{\perp}T_{e1}^{\perp} - (m_e n_0/\tau_{ee})(1 - \bar{K}_{RR})u_{ei1z}, \tag{42}$$

where

$$\gamma_{ez}^{\|} = \frac{3}{5}\bar{K}_{hR} + \frac{1}{2}\bar{K}_{\sigma R} - \frac{4\bar{K}_{RS}}{3\bar{k}_{\|}}, \tag{43}$$

$$\gamma_{ez}^{\perp} = \frac{2}{5}\bar{K}_{hR} - \frac{1}{2}\bar{K}_{\sigma R} + \frac{4\bar{K}_{RS}}{3\bar{k}_{\|}}. \tag{44}$$

The x component of $\mathbf{R}_{e1}$ is[26]

$$R_{e1}^{\perp} = -\alpha^{\perp}\frac{m_e n_0}{\tau_{ei}}u_{ei1x} - \alpha^{\perp}\frac{m_e u_{e0x}}{\tau_{ei}}n_{e1} - ik_{\perp}\beta^{\perp}n_0 T_{e1}, \tag{45}$$

where $\beta^{\perp}$ for $Z_i = 1$ is given by[26]

$$\beta^{\perp} = \frac{6.33r + 2.47}{r^{\frac{8}{3}} + 2.75r^{\frac{7}{3}} + 3.99r^2 + 5.31r^{\frac{5}{3}} + 8.23r + 3.52}. \tag{46}$$

Finally, the y component of $\mathbf{R}_{e1}$ is given by $R_{e1}^{\times} = \alpha^{\times} m_e n_0 u_{ei1y}/\tau_{ei}$. Here, the coefficient $\alpha^{\times}$ for $Z_i = 1$ is[26]

$$\alpha^{\times} = \frac{r(2.53r + 0.81)}{r^{\frac{8}{3}} + 2.54r^{\frac{7}{3}} + 6.14r^2 + 7.35r^{\frac{5}{3}} + 11.22r + 4.09}. \tag{47}$$

With these closures, the first-order momentum equation [Eq. (8)] can be used to obtain the perturbed electron current density $\mathbf{J}_{e1}$. Then, the Maxwell equation [Eq. (5)] can be written as

$$\begin{pmatrix} D_{xx} & D_{xy} & D_{xz} \\ D_{yx} & D_{yy} & D_{yz} \\ D_{zx} & D_{zy} & D_{zz} \end{pmatrix} \begin{pmatrix} E_{1x} \\ E_{1y} \\ E_{1z} \end{pmatrix} = 0. \tag{48}$$

The detailed derivation of each component of tensor $\mathbf{D}$ can be found in Appendix B.

III. COLLISIONAL EFFECTS ON THE DISPERSION

Dispersion relations for the lower hybrid drift waves are obtained from $|\mathbf{D}| = 0$, where $|\mathbf{D}|$ is the determinant of the tensor $\mathbf{D}$; from this equation, the normalized angular frequency Ω is computed numerically for the given $\mathbf{k}$ and θ. Required input parameters are B_0, n_0, T_{e0}, T_{i0}, u_{e0z}, and u_{e0x}. In addition, the ion mass has to be specified.

Compared to the previous collisionless model in Yoo *et al.*,[7] there are two significant changes in the current model: the inclusion of the first-order perturbation of the perpendicular electron temperature ($T_{e1}^{\perp}$) and the use of collisional closures. To understand the effects of each change, we obtain dispersion relations from four different models—(i) the collisionless model in Ref. Yoo *et al.*,[7] (ii) a model with collisional closures but without $T_{e1}^{\perp}$, (iii) the current model in the collisionless limit $\tau_{ee} \to \infty$, and (iv) the current model.

First, we obtain dispersion relations with typical plasma and field parameters near the electron diffusion region of the MRX during reconnection with a guide field; $B_0 = 180$ Gauss, $n_0 = 2 \times 10^{13}\ \mathrm{cm}^{-3}$, $T_{e0} = T_{i0} = 10$ eV, $u_{e0z} = -130$ km/s, and $u_{e0x} = 50$ km/s. Here, the ion species is singly ionized helium. Justified by previous measurements in MRX,[19,31] we assume that $Z_i = 1$. With these parameters, $\tau_{ee}\omega_{ce} = 157$, β_e is 0.25 and V_A is 44 km/s. Note that u_{e0x} exceeds V_A, which is a necessary condition for LHDWs to have large growth rates.

Figure 2 shows dispersion relations from the four models. Left (right) panels are contour plots of the real (imaginary) part of the angular frequency as a function of $k\rho_e$ and θ. Here $\rho_e = v_{te}/\omega_{ce}$ is the electron gyroradius. From now on, ω represents the real part of the angular frequency and γ represents the imaginary part. Both ω and γ are normalized to the (angular) lower hybrid frequency, ω_{LH}. All four models are qualitatively similar, showing strong growth rates ($\gamma \lesssim 0.6\omega_{LH}$) for the ES-LHDW. The ES-LHDW propagates almost perpendicular to $\mathbf{B}_0$ ($\theta \sim 90°$) with $\omega \lesssim \omega_{LH}$. The peak growth rate occurs at $k\rho_e \sim 0.7$ and $\theta \sim 91°$. Here $k\rho_e \sim 0.7$ corresponds to $\lambda \sim 0.6$ cm. These similarities among the four models indicate that the effects of Coulomb collisions on the ES-LHDW are limited for typical MRX parameters. Moreover, inclusion of $T_{e1}^{\perp}$ also has a limited impact on the dispersion.

For a better comparison between the four models, the dispersion relation and growth rate of the ES-LHDW are presented in Fig. 3 for $\theta = 91°$. It is worth noting that including Coulomb collisions decreases the growth rate γ. This is understandable since collisions decrease the reaction of electrons to the external perturbation, such that they reduce the positive feedback from the plasma. The change in ω is not straightforward but is related to frequency shift due to additional terms of u_{e1x} and u_{e1z}. For example, the parallel force balance equation Eq. (B48) has the resistivity $R_{e1}^{||}$, which adds additional terms in α_{ez} in Eq. (B50). These additional terms can cause a shift in ω (note that α_{ez} has a dependency on ω via α_e).

It is interesting to see that including $T_{e1}^{\perp}$ in the electron dynamics decreases both ω and γ of the ES-LHDW. Interpreting this trend is complicated, because $T_{e1}^{\perp}$ impacts both the x and z components of the electron momentum equation. For the x component, the first term ($ik_\perp n_0 T_{e1}^{\perp}$) on the right side of Eq. (B55), which is the perturbed perpendicular electron pressure gradient term, directly contains $T_{e1}^{\perp}$. For the parallel momentum balance of Eq. (B48), $T_{e1}^{\perp}$ affects $T_{e1}^{||}$ via $q_{e1x}^{||}$ in Eq. (23). The parallel resistivity [Eq. (42)] also has a term with $T_{e1}^{\perp}$ ($-ik_{||} n_0 \gamma_{ez}^{\perp} T_{e1}^{\perp}$).

The dispersion relation is calculated after setting $\gamma_{ez}^{\perp} = 0$ to remove contributions from $T_{e1}^{\perp}$ in the z component of the electron force balance equation. As shown in Fig. 4, this change (green line) decreases ω and increases γ, compared to the reference case with $T_{e1}^{\perp}$ (red line). Changes in ω and γ are not significant.

The change in ω with $T_{e1}^{\perp}$ is caused by the $ik_\perp n_0 T_{e1}^{\perp}$ term in the x component of the electron momentum equation. As shown in Fig. 4(a), without the term (magenta line), ω increases significantly compared to the reference case with $T_{e1}^{\perp}$ (red line). Removing the $ik_\perp n_0 T_{e1}^{\perp}$ term also increases γ for most values of k. Again, these changes are caused by the frequency shift due to the additional term with u_{e1x}; from Eqs. (B35) and (B55), the inertial term effectively changes from $im_e n_0(\omega - \mathbf{k}\cdot\mathbf{u}_{e0})u_{e1x}$ to $im_e n_0(\omega - \mathbf{k}\cdot\mathbf{u}_{e0} - 0.5\bar{c}_{ux}^{\perp} k_\perp v_{te})u_{e1x}$.

We have repeated the dispersion calculation for the EM-LHDW that propagates obliquely to $\mathbf{B}_0$. The plasma and field parameters used for calculations are $B_0 = 30$ Gauss, $n_0 = 2 \times 10^{13}\ \mathrm{cm}^{-3}$, $T_{e0} = T_{i0} = 10$ eV, $u_{e0z} = -50$ km/s, and $u_{e0x} = 130$ km/s. Again, the ion species is singly ionized helium and $Z_i = 1$. With these parameters, $\tau_{ee}\omega_{ce} = 26.2$, β_e is 8.9 and V_A is 7.3 km/s. These parameters represent typical MRX values near the electron diffusion region during reconnection with a negligible guide field.

As shown in Fig. 5, dispersion relations from the four models again qualitatively agree with each other; these models expect positive growth rates for the EM-LHDW. Models without $T_{e1}^{\perp}$ have the maximum growth rate around $k\rho_e \sim 0.6$ and $\theta \sim 55°$, while those with $T_{e1}^{\perp}$ have the maximum growth rate around $k\rho_e \sim 0.5$ and $\theta \sim 50°$. The wavelength with the largest growth rate is about 4 cm. In is interesting to see that all models expect that the mode has frequency significantly less than ω_{LH} in the ion rest frame. This agrees with measurements in MRX and numerical simulations that show that most of the power of the EM-LHDW exists below ω_{LH}.[9,16]

For comparison between the four models, ω and γ as a function of k for $\theta = 55°$ are presented in Fig. 6. Similar to the ES-LHDW case, collisional effects decrease γ regardless of the existence of $T_{e1}^{\perp}$ in the model. This is consistent with the aforementioned explanation; collisions decrease the reaction of electrons to the external perturbation, thereby decreasing the positive feedback. For the EM-LHDW, collisions generally decrease ω especially when $T_{e1}^{\perp}$ is not included in the model (blue lines). Including $T_{e1}^{\perp}$ further decreases both ω and γ for this mode (red lines).

IV. SUMMARY AND DISCUSSION

In summary, we have developed a local, linear model of LHDWs that includes effects of Coulomb collisions and $T_{e1}^{\perp}$. This model works best for plasmas with weak collisionality. Without collisions, some assumptions for the 3 + 1 model may not be valid, as the zeroth-order

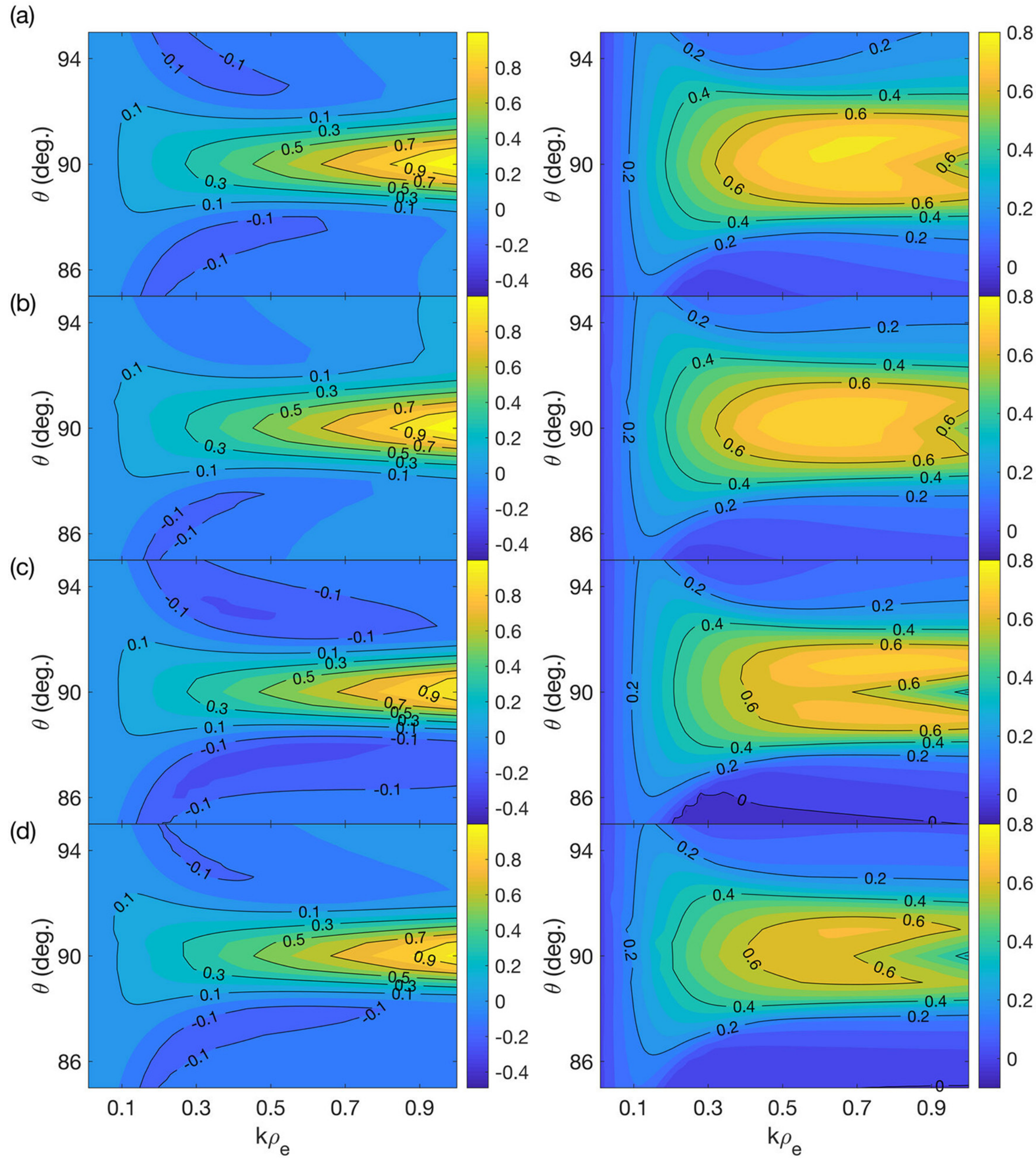

FIG. 2. Dispersion relation of the LHDW with typical MRX parameters near the electron diffusion region with a high guide field. Left (right) panels show the real (imaginary) part of the angular frequency as a function of k and θ. (a) Collisionles model without $T_{e1}^{\perp}$. (b) Collisional model without $T_{e1}^{\perp}$. (c) Model with $T_{e1}^{\perp}$ in the collisionless limit ($\tau_{ee} \to \infty$). (d) Collisional model with $T_{e1}^{\perp}$ (the most complete model). The results from the four models qualitatively agree with each other; the quasi-electrostatic LHDW that propagates almost perpendicular to $\mathbf{B}_0$ is unstable. The maximum growth rate appears around $k\rho_e \sim 0.7$ and $\theta \sim 91°$. The growth rate of the mode decreases with the collisional effects (b) and (d), compared to the corresponding collisionless cases (a) and (c).

distribution function is not close to a Maxwellian. In addition, in the collisionless plasma, agyrotropy can be developed, while a gyrotropic electron pressure tensor is assumed in this model. For collisional plasmas, we need to consider the zeroth-order electric field along the x and z directions; for the zeroth-order electron force balance, additional components of $\mathbf{E}_0$ are needed to balance the zeroth-order resistivity $\mathbf{R}_{e0}$. If there are too many collisions, we need additional first-order terms ($eE_{0x}n_{e1}$ and $eE_{0z}n_{e1}$) in the x and z components of the electron momentum equation [Eq. (8)]. From Eq. (38), required equilibrium electric field components are given by $E_{0z} = -\alpha^{\|}B_0 u_{e0z}/\omega_{ce}\tau_{ei}$ and $E_{0x} = -\alpha^{\perp}B_0 u_{e0x}/\omega_{ce}\tau_{ei}$. From Eq. (3), E_{0x}/E_0 is given by

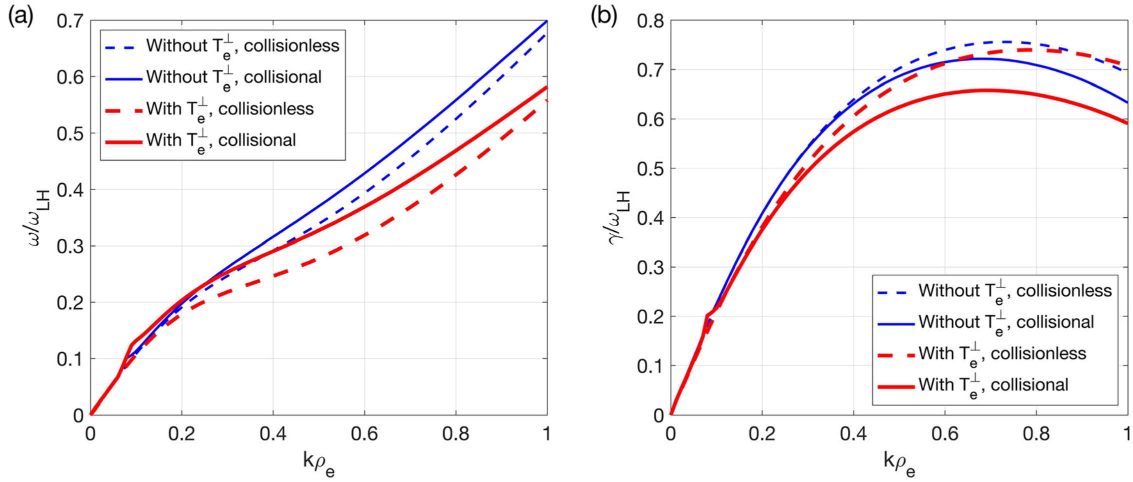

FIG. 3. 1D dispersion relation of the ES-LHDW for $\theta = 91°$. (a) $\omega/\omega_{\rm LH}$ as a function of $k\rho_{\rm e}$. Including the collisional effects (solid lines) increases the real frequency, while models with $T_{\rm e1}^{\perp}$ (red lines) have lower ω. (b) $\gamma/\omega_{\rm LH}$ as a function of $k\rho_{\rm e}$. Collisional effects (solid lines) decrease γ, compared to the results from the corresponding collisionless cases (dashed lines).

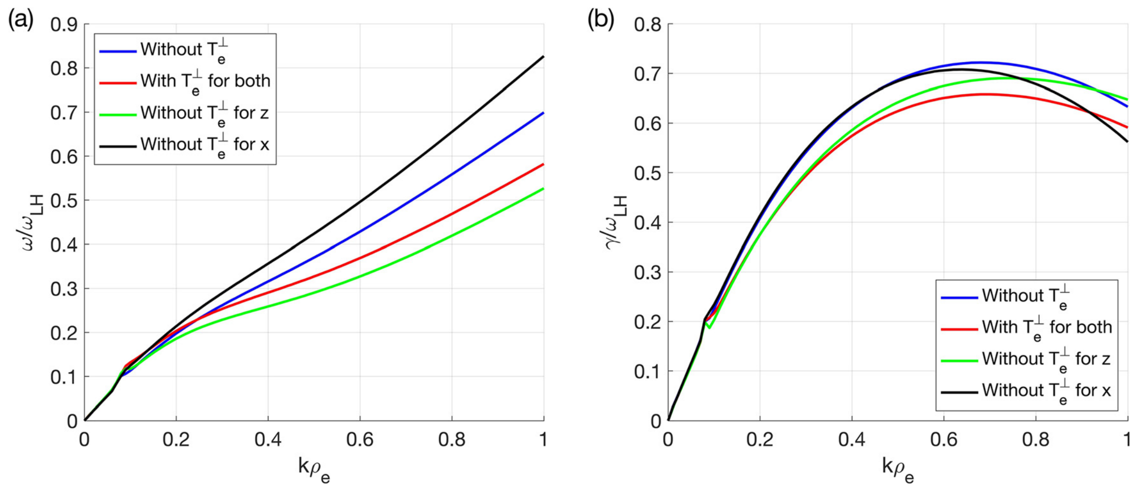

FIG. 4. 1D dispersion relation of the ES-LHDW for $\theta = 91°$. (a) $\omega/\omega_{\rm LH}$ as a function of $k\rho_{\rm e}$ for four cases with collisional effects. The blue (red) line indicates the reference case without (with) $T_{\rm e1}^{\perp}$. If $T_{\rm e1}^{\perp}$ is removed from the *x* component of the electron momentum equation (cyan line), ω becomes significantly larger. Removing the contribution from $T_{\rm e1}^{\perp}$ in the *z* component of the electron momentum equation (green line), on the other hand, reduces ω. (b) $\gamma/\omega_{\rm LH}$ as a function of $k\rho_{\rm e}$ for four cases with collisional effects. Effects of $T_{\rm e1}^{\perp}$ on γ are not important, as all four cases show similar values.

$$\frac{E_{0x}}{E_0} = -\frac{\alpha^{\perp} T_{\rm e0}}{T_{\rm e0}+T_{\rm i0}}\frac{1}{\omega_{\rm ce}\tau_{\rm ei}} \sim -\frac{1}{\omega_{\rm ce}\tau_{\rm ee}}, \tag{49}$$

because $\alpha_{\perp} \sim T_{\rm e0}/(T_{\rm e0}+T_{\rm i0}) \sim 1$ and $\tau_{\rm ei} \sim \tau_{\rm ee}$ for $Z_{\rm i} = 1$. This means that E_{0x} is negligible compared to E_0, as long as electrons are fully magnetized ($\omega_{\rm ce}\tau_{\rm ee} \gg 1$), which is one of the basic assumptions of this model. From a similar argument, E_{0z} is also negligible unless $|u_{\rm e0z}| \gg |u_{\rm e0x}|$. For the two cases presented here, the effects of both E_{0x} and E_{0z} are expected to be minimal since $|u_{\rm e0z}| \sim |u_{\rm e0x}|$ and $\omega_{\rm ce}\tau_{\rm ee} \gg 1$.

To verify this argument, we have calculated dispersion relations of LHDWs after including two additional terms ($eE_{0x}n_{\rm e1}$ and $eE_{0z}n_{\rm e1}$) and have found that impacts from these terms are actually negligible. The basic reason for not including additional components of $\mathbf{E}_0$ in the current model is that including E_{0x} may require an additional electron flow component along the *y* direction, since there will be a corresponding $\mathbf{E}\times\mathbf{B}$ drift of electrons, while ions are unmagnetized. This means that collisions may impact the dynamics of LHDWs by changing the equilibrium itself. A future work will address this effect in a self-consistent manner. As the main purpose of the current study is to study collisional effects on LHDWs, we minimize other changes for simplicity. The parallel component of the equilibrium electric field E_{0z}, on the other hand, can be easily added in the model without creating complexity. Moreover, E_{0z} in the electron diffusion region during

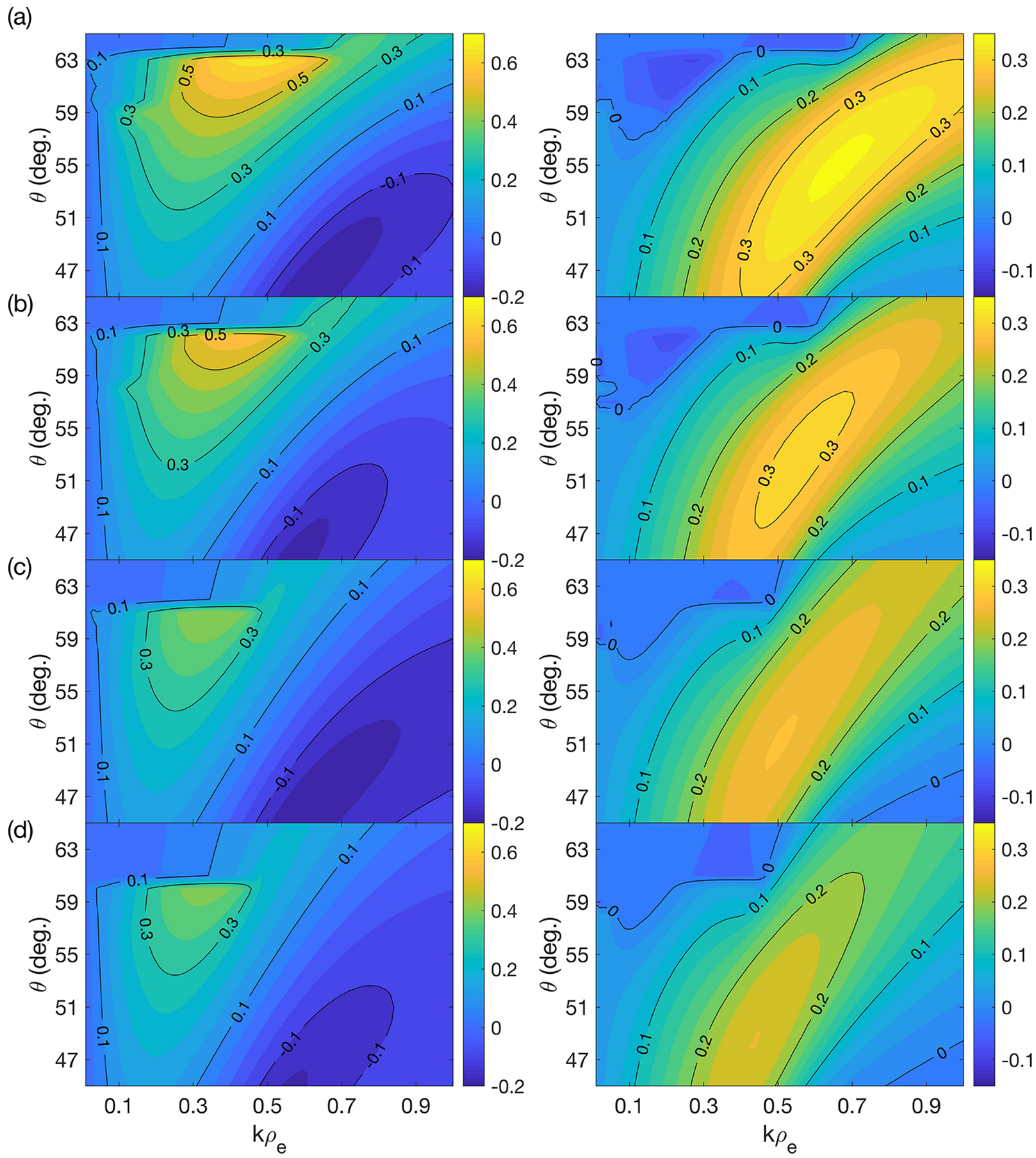

FIG. 5. Dispersion relation of the LHDW with typical MRX parameters near the electron diffusion region with a negligible guide field. Left (right) panels show the real (imaginary) part of the angular frequency as a function of k and θ. (a) Collisionless model without $T_{e1}^{\perp}$. (b) Collisional model without $T_{e1}^{\perp}$. (c) Model with $T_{e1}^{\perp}$ in the collisionless limit ($\tau_{ee} \rightarrow \infty$). (d) Collisional model with $T_{e1}^{\perp}$ (the most complete model). Again, the results from the four models qualitatively agree with each other; the electromagnetic LHDW that propagates obliquely to $\mathbf{B}_0$ is unstable. The maximum growth rate appears around $k\rho_e \sim 0.5$ and $\theta \sim 50°$. The growth rate of the mode decreases with collisional effects (b) and (d), compared to the corresponding collisionless cases (a) and (c).

reconnection with a strong guide field may significantly exceed the value required to balance the classical resistivity.[32] In the future, we will study the possible impacts of E_{0z} on LHDWs with values measured in MRX during guide field reconnection.

With this model, we have calculated two sets of LHDW dispersion relations for typical MRX parameters. The first case uses parameters from the electron diffusion region during reconnection with a significant guide field, while the second one uses those with a negligible guide field. Due to the presence of the guide field, the first case has a low electron beta ($\beta_e = 0.25$), such that the ES-LHDW is unstable in that region. For the second case ($\beta_e = 8.9$), on the other hand, the ES-LHDW is stabilized by the high beta effect[17] and the EM-LHDW is unstable instead.

It will be interesting to study the critical value of β_e that determines whether the ES- or EM-LHDW is unstable. Initial studies show that the critical value is determined by the value of u_{e0x}/V_A; for a relatively low ($\sim$1) value of u_{e0x}/V_A like the first case, β_e also has to be low ($\lesssim$0.5) to have the ES-LHDW unstable. For a high value (>10) of

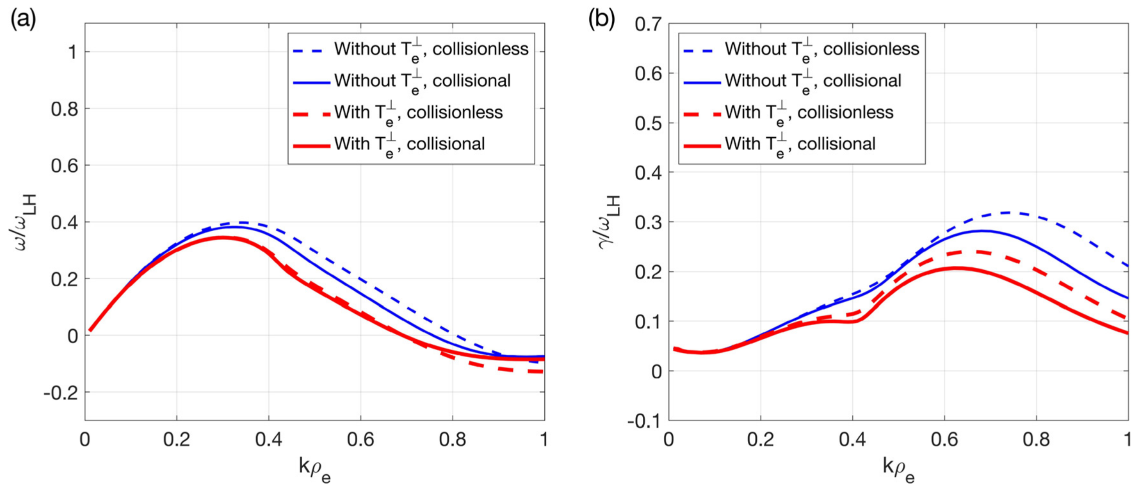

FIG. 6. 1D dispersion relation of the EM-LHDW for $\theta = 55°$. (a) ω/ω_{LH} as a function of $k\rho_e$. Models with $T_{e1}^{\perp}$ (red lines) have lower ω. The impact of Coulomb collisions on ω is negligible. (b)γ/ω_{LH} as a function of $k\rho_e$. Collisional effects (solid lines) decreases γ, compared to the results from the corresponding collisionless cases (dashed lines).

u_{e0x}/V_A, on the other hand, the ES-LHDW exists at the higher $\beta_e \sim 1$. We plan to conduct a statistical study with data from MMS and/or MRX, which will be compared to the results from the current theoretical model.

Based on the two cases we have studied, collisional effects on LHDWs in typical MRX current sheets are limited. In both cases, including Coulomb collisions in the model decreases the growth rate. However, the difference in γ is relatively small ($\lesssim$20%). This is because the wavelengths of LHDWs (0.5–5 cm) are smaller than the mean free path of electrons ($\sim$10 cm) and electrons are fully magnetized ($\omega_{ce}\tau_{ee} \gg 1$) for these parameters.

To further investigate how collisions may impact on the dispersion relation, we have artificially varied τ_{ee} and τ_{ei}. For the ES-LHDW, artificially high collisions significantly affect the dispersion relation and the growth rate, as shown in Figs. 7(a) and 7(b). When the collisions are enhanced by a factor of 5 (red dashed line), the real frequency becomes larger for $k\rho_e > 0.2$ than the reference value (blue solid line). There is also a significant decrease in the growth rate for $k\rho_e > 0.7$. Changes in less collisional cases, on the other hand (green solid and dashed lines), are minimal. With the reduced collision time ($\tau_{ee} \to 0.2\tau_{ee}$), the mean free path ($\tau_{ee}v_{te}$) becomes about 2 cm, which corresponds to $k\rho_e \sim 0.2$. This supports the insertion that collisions have large impacts on modes with a wavelength comparable to the mean free path ($\lambda \sim 2\pi\tau_{ee}v_{te}$).

For the case of the EM-LHDW, the effects from collisions become significant when collisions are enhanced by a factor of 5 or more ($\tau_{ee} \to 0.2\tau_{ee}$ and $\tau_{ei} \to 0.2\tau_{ei}$). As denoted by the red line in Fig. 7(c), the overall shape of the dispersion relation changes noticeably, when τ_{ee} is reduced to $0.2\tau_{ee}$. The mean free path with $0.2\tau_{ee}$ is about 2 cm (the same electron temperature and density as the first case), and the change starts around $0.2k\rho_e$. When τ_{ee} reduces even further to $0.1\tau_{ee}$ (red dashed line), the deviation from the reference line starts around $0.1k\rho_e$. For both cases, there are also significant reductions in γ, as shown in Fig. 7(d) especially for $k\rho_e < 0.7$.

This means that parameters for the two cases studied here are actually in the weakly collisional regime and that the dynamics of LHDWs are susceptible to collisional effects only when collisions are strong. For example, if the base electron temperature for both cases is 3 eV, the dispersion relation from this collisional model will be vastly different from that of the collisionless model.

Including $T_{e1}^{\perp}$ in the model has limited impacts on the dispersion; it generally decreases the frequency and growth rate of LHDWs, but changes in ω and γ are less than 20% for both cases. These changes mostly come from the additional pressure gradient term ($ik_{\perp}n_0T_{e1}^{\perp}$) in the electron momentum equation along the x direction. This limited impact is related to the existence of Lorentz force terms along the perpendicular direction;[7] because of these terms, the electron force balance is less sensitive to the pressure gradient term along the perpendicular direction.

It should be noted that the current theoretical model ignores the global structure of the current sheet by assuming that there is no wave propagation along the density gradient direction (y direction in Fig. 1). To address the effects from the global current sheet structure, an eigenmode analysis[21,33] or numerical simulations[22,23] will have to be carried out, which will be one of our future works. In MRX, where the current sheet is actually broader ($\sim 10d_e$; d_e is electron skin depth), this local approximation is generally valid, as the length scale along the y direction is larger than the wavelength of LHDWs.

This model assumes that there is no equilibrium temperature gradient across the current sheet. In MRX, electrons are locally heated in the current sheet.[20,34] However, inside the current sheet the temperature gradient is rather small, compared to that of density. Therefore, the effects of the temperature gradient are expected to be negligible.[24]

This study will provide a theoretical framework for quantifying anomalous terms and heating associated with LHDWs in MRX. With the solved dispersion relation, we can express every fluctuating quantity in terms of a measurable quantity. For example, the first-order density perturbation [Eq. (B81)] can be expressed in terms of the fluctuation in the reconnection electric field (δE_{rec}) that can be measured with a probe.[8,35] Then, the wave-associated anomalous drag term $D = -\langle \delta n_e \delta E_{rec}\rangle / \langle n_e \rangle$[36] can be estimated by measuring δE_{rec}. Here, the assumption is that the linear relation holds, such that we can use

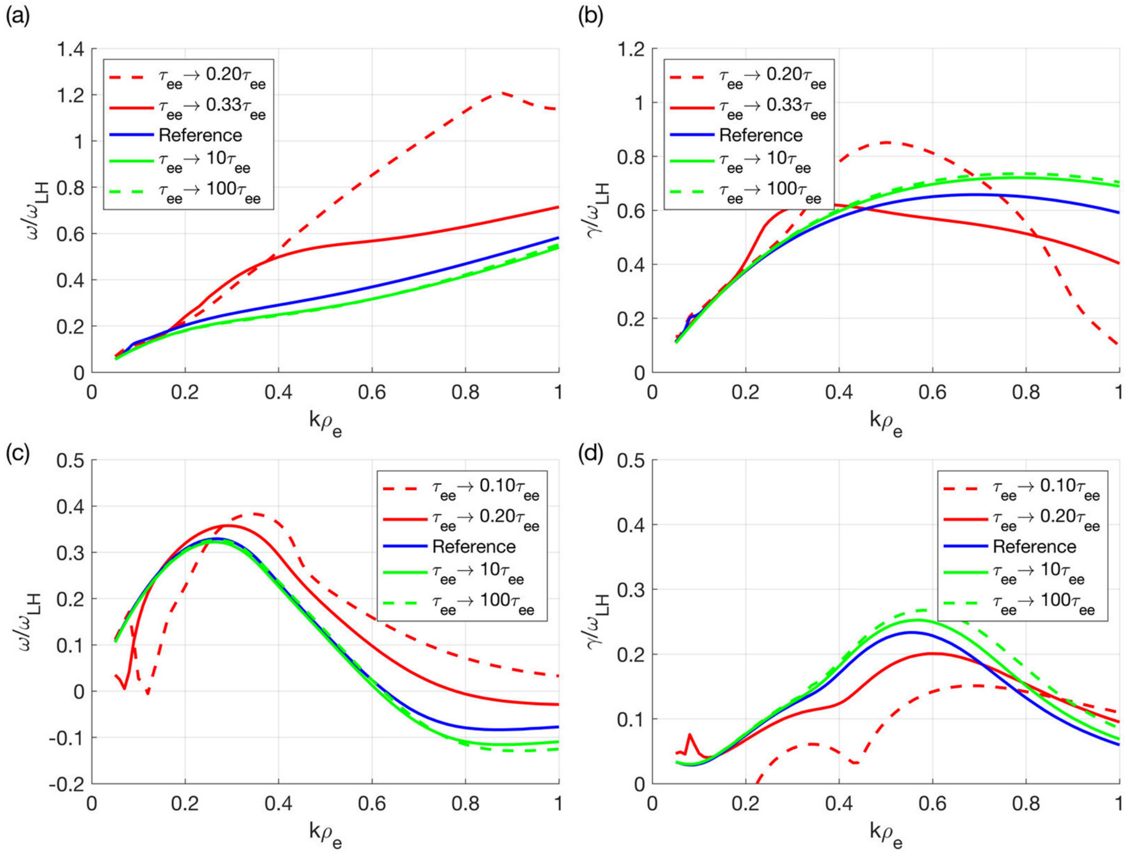

FIG. 7. 1D dispersion relations with various collisionalities for the two cases. (a) ω/ω_{LH} as a function of $k\rho_e$ for the ES-LHDW case. When τ_{ee} is artificially decreased to $0.2\tau_{ee}$ (red dashed line), which means that collisions are enhanced by a factor of 5, there is a significant increase in ω when $k\rho_e > 0.4$. The same change is also applied to the other collision time, τ_{ei}. The blue line indicates the reference value without any change in the collision time. (b)γ/ω_{LH} as a function of $k\rho_e$ for the ES-LHDW case. When collisions are enhanced (red solid and dashed lines), there are noticeable changes in γ. (c)ω/ω_{LH} as a function of $k\rho_e$ for the EM-LHDW case. When collisions are enhanced, there are large changes in the dispersion. (d)γ/ω_{LH} as a function of $k\rho_e$ for the EM-LHDW case. When collisions are enhanced (red solid and dashed lines), the growth rate with smaller $k\rho_e$ decreases notably.

$n_{e1} \sim \delta n_e$. Furthermore, this model can provide direct estimates of wave-associated heating in Eq. (35) via the same quasi-linear argument. This estimate cannot be done with other collisionless models. In the future, we will establish quasi-linear calculations and conduct measurements of LHDWs in MRX to find out how LHDWs affect the electron and reconnection dynamics.

ACKNOWLEDGMENTS

This work was supported by DOE Contract No. DE-AC0209CH11466, NASA Grant Nos. NNH20ZDA001N and 80HQTR21T0060, NNSFC Contract No. 11975163, the Priority Academic Program Development of Jiangsu Higher Education Institutions (PAPD), and a DOE Grant No. DE-FG02–04ER54746. Digital data used are available in the DataSpace of Princeton University (http://arks.princeton.edu/ark:/88435/dsp01x920g025r).

AUTHOR DECLARATIONS

Conflict of Interest

The authors have no conflicts to disclose.

DATA AVAILABILITY

The data that support the findings of this study are openly available in the DataSpace of Princeton University http://arks.princeton.edu/ark:/88435/dsp01b2773z812, Ref. 38.

APPENDIX A: DERIVATION OF THE HEAT FLUX CLOSURE

From the kinetic equation in the $(t, \mathbf{r}, \mathbf{w} \equiv \mathbf{v} - \mathbf{V})$ coordinates ($\mathbf{V}$ is the fluid velocity),

$$\frac{df}{dt} - (\mathbf{w}\cdot\nabla\mathbf{V})\cdot\frac{\partial}{\partial\mathbf{w}}f + \nabla\cdot(\mathbf{w}f) + \frac{\partial}{\partial\mathbf{w}}\cdot(\mathbf{A}f) + \frac{q}{m}\mathbf{w}\times\mathbf{B}\cdot\frac{\partial}{\partial\mathbf{w}}f = C(f), \tag{A1}$$

where

$$\frac{d}{dt} = \frac{\partial}{\partial t} + \mathbf{V}\cdot\nabla, \tag{A2}$$

$$\mathbf{A}=\frac{1}{m}[\mathbf{F}_*+q(\mathbf{V}\times\mathbf{B})]-\frac{d\mathbf{V}}{dt}. \tag{A3}$$

For the $p^{||}$ fluid equation, we need to obtain the closure,

$$\mathbf{q}^{||}=\int d^3v m w_{||}^2\mathbf{w}f=q_{||}^{||}\hat{z}+\mathbf{q}_{\perp}^{||}, \tag{A4}$$

$$\mathbf{q}=\mathbf{h}=\int d^3v\frac{1}{2}mw^2\mathbf{w}f=h_{||}\hat{z}+\mathbf{h}_{\perp}, \tag{A5}$$

where

$$q_{||}^{||}=\int d^3v m w_{||}^3 f=\frac{6}{5}h_{||}+\sigma_{||}, \tag{A6}$$

$$q_{||}^{\perp}=\int d^3v\frac{1}{2}mw_{\perp}^2 w_{||}f=\frac{2}{5}h_{||}-\frac{1}{2}\sigma_{||} \tag{A7}$$

have been obtained in Ji and Joseph,[25] and the $\mathbf{q}_{\perp}^{||}$ has been obtained in Yoo *et al.*[7] Now we obtain

$$\mathbf{q}^{\perp}=\int d^3v\frac{1}{2}mw_{\perp}^2\mathbf{w}f=q_{||}^{\perp}\hat{z}+\mathbf{q}_{\perp}^{\perp}. \tag{A8}$$

Note that $\mathbf{q}^{\perp}$ can be obtained from

$$\mathbf{h}_{\perp}=\mathbf{q}_{\perp}=\int d^3v\frac{1}{2}mw^2\mathbf{w}_{\perp}f=\frac{1}{2}\mathbf{q}_{\perp}^{||}+\mathbf{q}_{\perp}^{\perp}. \tag{A9}$$

We adopt the closure (transport) ordering $d/dt\approx 0$ and the linear response theory, linear in thermodynamic drives, i.e., ∇T, $\nabla p_{||}$ and $\nabla p_{\perp}$.

We take the moments $\int d^3v\frac{1}{2}mw^2\mathbf{w}$ of the kinetic equation:

$$\int d^3v\frac{1}{2}mw^2\mathbf{w}\frac{df}{dt}=\frac{d}{dt}\mathbf{q}\ :\ \text{ignored by the closure ordering,}$$

$$\int d^3v\frac{1}{2}mw^2\mathbf{w}(\mathbf{w}\cdot\nabla\mathbf{V})\cdot\frac{\partial}{\partial\mathbf{w}}f\ :\ \text{ignored by the linearization,}$$

$$\int d^3v\frac{1}{2}mw^2\mathbf{w}\nabla\cdot(\mathbf{w}f)=\nabla\cdot\left(\int d^3v\frac{1}{2}mw^2\mathbf{w}\mathbf{w}f\right).$$

We should decompose $\mathbf{wwww}$ into orthogonal polynomials (see Ji and Held[37]) for the consistent truncation in the expansion of a distribution function.

$$\mathbf{c}=\frac{\mathbf{w}}{v_T}=\frac{\mathbf{w}}{\sqrt{2T/m}}. \tag{A10}$$

In terms of orthogonal basis

$$\begin{aligned}
c^2\mathbf{cc}&=c^2\left(\mathbf{cc}-\frac{1}{3}c^2\mathsf{I}\right)+\frac{1}{3}c^4\mathsf{I}\\
&=\left(c^2-\frac{7}{2}\right)\left(\mathbf{cc}-\frac{1}{3}c^2\mathsf{I}\right)+\frac{7}{2}\left(\mathbf{cc}-\frac{1}{3}c^2\mathsf{I}\right)+\frac{1}{3}c^4\mathsf{I}\\
&=-\mathsf{p}^{21}+\frac{7}{2}\mathsf{p}^{20}+\frac{2}{3}\left(\frac{1}{2}c^4-\frac{5}{2}c^2+\frac{15}{8}\right)\mathsf{I}+\frac{2}{3}\left(\frac{5}{2}c^2-\frac{15}{8}\right)\mathsf{I}\\
&=-\mathsf{p}^{21}+\frac{7}{2}\mathsf{p}^{20}+\frac{2}{3}\mathsf{p}^{02}\mathsf{I}+\left[\frac{5}{3}\left(c^2-\frac{3}{2}\right)+\frac{5}{2}-\frac{5}{4}\right]\mathsf{I}\\
&=-\mathsf{p}^{21}+\frac{7}{2}\mathsf{p}^{20}+\frac{2}{3}\mathsf{p}^{02}\mathsf{I}+\left(-\frac{5}{3}\mathsf{p}^{01}+\frac{5}{4}\right)\mathsf{I},
\end{aligned} \tag{A11}$$

$$\begin{aligned}
\int d\mathbf{v}\frac{1}{2}mw^2\mathbf{ww}f&\rightarrow\frac{1}{2}mv_T^4\left[\frac{7}{2}\mathsf{p}^{20}+\left(-\frac{5}{3}\mathsf{p}^{01}+\frac{5}{4}\right)\mathsf{I}\right]\\
&=\frac{7}{2}\frac{1}{2}v_T^2\boldsymbol{\pi}+\frac{1}{2}mv_T^4\frac{5}{4}n\mathsf{I}\\
&=\frac{7}{2}\frac{T}{m}\boldsymbol{\pi}+\frac{5}{2}\frac{T}{m}p\mathsf{I}\\
&=\frac{7}{2}\frac{T}{m}\mathsf{p}-\frac{T}{m}p\mathsf{I}.
\end{aligned} \tag{A12}$$

Hereafter $\rightarrow$ will be used to drop $\mathbf{b}$ terms, which will be nullified by the $\mathbf{b}\times$ operation,

$$\nabla\cdot\boldsymbol{\pi}=\frac{3}{2}\mathbf{b}\partial_{||}\pi_{||}-\frac{1}{2}\nabla\pi_{||}\rightarrow-\frac{1}{2}\nabla\pi_{||}. \tag{A13}$$

For the $\frac{\partial}{\partial\mathbf{w}}\cdot(\mathbf{A}f)$ term

$$\mathbf{A}=\frac{1}{m}[\mathbf{F}_*+q(\mathbf{V}\times\mathbf{B})]-\frac{d\mathbf{V}}{dt}=\frac{1}{mn}(\nabla p+\nabla\cdot\boldsymbol{\pi}). \tag{A14}$$

$$\begin{aligned}
\int d\mathbf{v}\frac{1}{2}mw^2\mathbf{w}\frac{\partial}{\partial\mathbf{w}}\cdot(\mathbf{A}f)&=-\int d\mathbf{v}m\mathbf{A}\cdot\frac{\partial}{\partial\mathbf{w}}\left(\frac{1}{2}w^2\mathbf{w}\right)f\\
&=-\int d\mathbf{v}m\left(\mathbf{A}\cdot\mathbf{ww}+\frac{1}{2}w^2\mathbf{A}\right)f\\
&=-\mathsf{p}\cdot\mathbf{A}-\frac{3}{2}p\mathbf{A}\\
&=-\mathbf{A}\cdot\boldsymbol{\pi}-\frac{5}{2}p\mathbf{A}.
\end{aligned} \tag{A15}$$

All together $\nabla\cdot(\mathbf{w}f)+\frac{\partial}{\partial\mathbf{w}}\cdot(\mathbf{A}f)$

$$\begin{aligned}
\mathbf{all}=&\nabla\cdot\left(\frac{7}{2}\frac{T}{m}\boldsymbol{\pi}+\frac{5}{2}\frac{T}{m}p\mathsf{I}\right)-\frac{1}{mn}(\nabla p+\nabla\cdot\boldsymbol{\pi})\cdot\boldsymbol{\pi}\\
&-\frac{5}{2}p\frac{1}{mn}(\nabla p+\nabla\cdot\boldsymbol{\pi})\\
=&\frac{7}{2m}(\nabla T\cdot\boldsymbol{\pi}+\underline{T\nabla\cdot\boldsymbol{\pi}_1})+\frac{5}{2m}\left(p\nabla T+\underline{T\nabla p_0}\right)\\
&-\frac{1}{mn}(\nabla p+\nabla\cdot\boldsymbol{\pi})\cdot\boldsymbol{\pi}-\frac{5}{2}p\frac{1}{mn}\left(\underline{\nabla p_0}+\underline{\nabla\cdot\boldsymbol{\pi}_1}\right)\\
=&\frac{7}{2m}\nabla T\cdot\boldsymbol{\pi}+\frac{1}{m}T\nabla\cdot\boldsymbol{\pi}+\frac{5}{2m}p\nabla T-\frac{1}{mn}(\nabla p+\nabla\cdot\boldsymbol{\pi})\cdot\boldsymbol{\pi},
\end{aligned} \tag{A16}$$

$$\begin{aligned}
\int d^3v\frac{1}{2}mw^2\mathbf{w}\frac{\partial}{\partial\mathbf{w}}\cdot(\mathbf{w}\times\mathbf{B}f)&=-\frac{1}{2}m\int d^3v(\mathbf{w}\times\mathbf{B}f)\cdot\frac{\partial}{\partial\mathbf{w}}(w^2\mathbf{w})\\
&=-\frac{1}{2}m\int d^3v(\mathbf{w}\times\mathbf{B}f)\cdot(2\mathbf{ww}+w^2\mathsf{I})\\
&=-\frac{1}{2}m\int d^3v w^2\mathbf{w}\times\mathbf{B}f\\
&=-\mathbf{h}\times\mathbf{B},
\end{aligned} \tag{A17}$$

$$\frac{q}{m}\int d^3v\frac{1}{2}mw^2\mathbf{w}\frac{\partial}{\partial\mathbf{w}}\cdot(\mathbf{w}\times\mathbf{B}f)=-\Omega\mathbf{h}\times\hat{z}. \tag{A18}$$

The final equation becomes up to $\mathcal{O}(\Omega^0)$

$$\begin{aligned}
&(\text{terms dropped by closure ordering})+\mathbf{all}+(\text{terms }\propto\mathbf{b})\\
&-\Omega\mathbf{h}\times\hat{z}=(\text{collision terms }\propto\mathbf{b})
\end{aligned}$$

$$\mathbf{h}_{\perp}=\frac{1}{\Omega}\hat{z}\times\mathbf{all}$$

$$\mathbf{h}_\perp = \frac{1}{m\Omega}\mathbf{b}\times\left[\frac{5}{2m}\nabla T\cdot\boldsymbol{\pi} + \frac{1}{m}T\nabla\cdot\boldsymbol{\pi} + \frac{5}{2m}p\nabla T - \frac{1}{mn}(\nabla\cdot\boldsymbol{\pi})\cdot\boldsymbol{\pi}\right]. \tag{A19}$$

Since we are interested in $\mathbf{q}_\perp$ up to $\mathscr{O}(\Omega^{-1})$, we consider only the CGL viscosity, which is $\mathscr{O}(\Omega^0)$

$$\boldsymbol{\pi} = \frac{3}{2}\pi_{||}\left(\mathbf{bb} - \frac{1}{3}\mathsf{I}\right), \tag{A20}$$

$$\nabla\cdot\boldsymbol{\pi} = \frac{3}{2}\mathbf{b}\partial_{||}\pi_{||} - \frac{1}{2}\nabla\pi_{||} = -\frac{1}{2}\nabla\pi_{||} + \mathbf{b}\text{ terms} \tag{A21}$$

and

$$(\nabla\cdot\boldsymbol{\pi})\cdot\boldsymbol{\pi} = \left(\frac{3}{2}\mathbf{b}\partial_{||}\pi_{||} - \frac{1}{2}\nabla\pi_{||}\right)\cdot\frac{3}{2}\pi_{||}\left(\mathbf{bb} - \frac{1}{3}\mathsf{I}\right) = \frac{1}{4}\pi_{||}\nabla\pi_{||} + \mathbf{b}\text{ terms}, \tag{A22}$$

$$\begin{aligned}\mathbf{all} &= \frac{7}{2m}\nabla T\cdot\boldsymbol{\pi} + \frac{1}{m}T\nabla\cdot\boldsymbol{\pi} + \frac{5}{2m}p\nabla T - \frac{1}{mn}(\nabla p + \nabla\cdot\boldsymbol{\pi})\cdot\boldsymbol{\pi}\\ &= -\frac{7}{4m}\pi_{||}\nabla T - \frac{T}{2m}\nabla\pi_{||} + \frac{5}{2m}p\nabla T + \frac{\pi_{||}}{2mn}\nabla p\\ &\quad - \frac{1}{4mn}\pi_{||}\nabla\pi_{||} + \mathbf{b}\text{ terms},\end{aligned} \tag{A23}$$

$$\mathbf{q}_\perp = \frac{1}{m\Omega}\mathbf{b}\times\left(-\frac{7}{4}\pi_{||}\nabla T - \frac{T}{2}\nabla\pi_{||} + \frac{5}{2}p\nabla T + \frac{\pi_{||}}{2n}\nabla p - \frac{1}{4n}\pi_{||}\nabla\pi_{||}\right), \tag{A24}$$

$$\mathbf{q}_\perp^\perp = \mathbf{q}_\perp - \frac{1}{2}\mathbf{q}_\perp^{||}, \tag{A25}$$

where[7]

$$\mathbf{q}_\perp^{||} = \frac{1}{m\Omega}\mathbf{b}\times\left(p^{||}\nabla T + T\nabla p^{||} - \frac{T}{2}\nabla\pi_{||} - \frac{p^{||}}{n}\nabla p^\perp\right). \tag{A26}$$

Finally,

$$\mathbf{q}^\perp = q_{||}^\perp\hat{z} + \mathbf{q}_\perp^\perp. \tag{A27}$$

One can rewrite equations in terms of $p^{||}$ and $p^\perp$ using

$$\pi_{||} = \frac{2}{3}(p^{||} - p^\perp), \tag{A28}$$

$$p = \frac{1}{3}\left(p^{||} + 2p^\perp\right) = nT. \tag{A29}$$

APPENDIX B: DERIVATION OF TENSOR D

In terms of $T_{e1}^{||}$ and $T_{e1}^\perp$, $q_{e1z}^{||}$ and $q_{e1z}^\perp$ [Eqs. (26) and (27)] can be expressed as

$$q_{e1z}^{||} = -i\bar{c}_{q||}^{||}n_0 v_{te}T_{e1}^{||} - i\bar{c}_{q\perp}^{||}n_0 v_{te}T_{e1}^\perp + \bar{c}_{qu}^{||}n_0 T_{e0}u_{ei1z}, \tag{B1}$$

$$q_{e1z}^\perp = -i\bar{c}_{q||}^\perp n_0 v_{te}T_{e1}^{||} - i\bar{c}_{q\perp}^\perp n_0 v_{te}T_{e1}^\perp + \bar{c}_{qu}^\perp n_0 T_{e0}u_{ei1z}, \tag{B2}$$

where six dimensionless parameters are defined as

$$\bar{c}_{q||}^{||} = \frac{9}{25}\bar{k}_{||}\bar{K}_{hh} - \frac{8}{5}\bar{k}_{||}\bar{K}_{h\sigma} + \frac{2}{3}\bar{k}_{||}\bar{K}_{\sigma\sigma} - \frac{4}{5}\bar{K}_{hS} - \frac{2}{3}\bar{K}_{\sigma S}, \tag{B3}$$

$$\bar{c}_{q\perp}^{||} = \frac{6}{25}\bar{k}_{||}\bar{K}_{hh} + \frac{4}{15}\bar{k}_{||}\bar{K}_{h\sigma} - \frac{2}{3}\bar{k}_{||}\bar{K}_{\sigma\sigma} + \frac{4}{5}\bar{K}_{hS} + \frac{2}{3}\bar{K}_{\sigma S}, \tag{B4}$$

$$\bar{c}_{qu}^{||} = \frac{6}{5}\bar{K}_{hR} + \bar{K}_{\sigma R}, \tag{B5}$$

$$\bar{c}_{q||}^\perp = \frac{3}{25}\bar{k}_{||}\bar{K}_{hh} + \frac{2}{15}\bar{k}_{||}\bar{K}_{h\sigma} - \frac{1}{3}\bar{k}_{||}\bar{K}_{\sigma\sigma} - \frac{4}{15}\bar{K}_{hS} + \frac{1}{3}\bar{K}_{\sigma S}, \tag{B6}$$

$$\bar{c}_{q\perp}^\perp = \frac{2}{25}\bar{k}_{||}\bar{K}_{hh} + \frac{8}{15}\bar{k}_{||}\bar{K}_{h\sigma} + \frac{1}{3}\bar{k}_{||}\bar{K}_{\sigma\sigma} + \frac{4}{15}\bar{K}_{hS} - \frac{1}{3}\bar{K}_{\sigma S}, \tag{B7}$$

$$\bar{c}_{qu}^\perp = \frac{2}{5}\bar{K}_{hR} - \frac{1}{2}\bar{K}_{\sigma R}. \tag{B8}$$

Here, $u_{ei1z} = u_{e1z} - u_{i1z}$ is the first-order relative flow velocity along the z direction.

With Eqs. (7), (9), (37), (38), (42), and (45), Q_{e1} can be written as

$$Q_{e1} = \left(1 - \bar{K}_{RR} + \frac{\alpha^{||}\tau_{ee}}{\tau_{ei}}\right)\frac{n_0 m_e u_{e0z}}{\tau_{ee}}u_{ei1z} + \frac{\bar{c}_{Q||}n_0}{\tau_{ee}}T_{e1}^{||} + \frac{\bar{c}_{Q\perp}n_0}{\tau_{ee}}T_{e1}^\perp + A_Q, \tag{B9}$$

where

$$\bar{c}_{Q||} = -\frac{m_e\tau_{ee}}{m_i\tau_{ei}} + \frac{i\bar{k}_{||}u_{e0z}}{v_{te}}\left(\frac{3\bar{K}_{hR}}{5} + \frac{\bar{K}_{\sigma R}}{2} - \frac{4\bar{K}_{RS}}{3\bar{k}_{||}}\right) + \frac{i\bar{k}_\perp\beta^\perp u_{e0x}}{3v_{te}}, \tag{B10}$$

$$\bar{c}_{Q\perp} = -\frac{2m_e\tau_{ee}}{m_i\tau_{ei}} + \frac{i\bar{k}_{||}u_{e0z}}{v_{te}}\left(\frac{2\bar{K}_{hR}}{5} - \frac{\bar{K}_{\sigma R}}{2} + \frac{4\bar{K}_{RS}}{3\bar{k}_{||}}\right) + \frac{2i\bar{k}_\perp\beta^\perp u_{e0x}}{3v_{te}}, \tag{B11}$$

$$A_Q = \left[\frac{3m_e(T_{i0} - T_{e0})}{m_i\tau_{ei}} + \frac{\alpha^\perp m_e u_{e0x}^2}{\tau_{ei}}\right]n_{e1} + \frac{3m_e n_0}{m_i\tau_{ei}}T_{i1} + \frac{2\alpha^\perp m_e n_0.u_{e0x}}{\tau_{ei}}u_{ei1x}. \tag{B12}$$

With Eqs. (32)–(34), and (B9), $C_{e1}^{||}$ and $C_{e1}^\perp$ can be written as

$$C_{e1}^{||} = \bar{c}_{C||}^{||}\frac{n_0 T_{e1}^{||}}{\tau_{ee}} + \bar{c}_{C\perp}^{||}\frac{n_0 T_{e1}^\perp}{\tau_{ee}} + \bar{c}_{Cu}^{||}\frac{n_0 T_{e0}u_{ei1z}}{\tau_{ee}v_{te}} + \frac{2}{3}A_Q, \tag{B13}$$

$$C_{e1}^\perp = \bar{c}_{C||}^\perp\frac{n_0 T_{e1}^{||}}{\tau_{ee}} + \bar{c}_{C\perp}^\perp\frac{n_0 T_{e1}^\perp}{\tau_{ee}} + \bar{c}_{Cu}^\perp\frac{n_0 T_{e0}u_{ei1z}}{\tau_{ee}v_{te}} + \frac{2}{3}A_Q, \tag{B14}$$

where six dimensionless parameters are given by

$$\bar{c}_{C||}^{||} = \frac{2}{3}\bar{c}_{Q||} + \frac{4}{5}\bar{k}_{||}\bar{K}_{hS} + \frac{2}{3}\bar{k}_{||}\bar{K}_{\sigma S} - \frac{2(2.05 - \bar{K}_{SS})}{3}, \tag{B15}$$

$$\bar{c}_{C\perp}^{||} = \frac{2}{3}\bar{c}_{Q\perp} + \frac{8}{15}\bar{k}_{||}\bar{K}_{hS} - \frac{2}{3}\bar{k}_{||}\bar{K}_{\sigma S} + \frac{2(2.05 - \bar{K}_{SS})}{3}, \tag{B16}$$

$$\bar{c}_{Cu}^{||} = \frac{4}{3}\left(1 - \bar{K}_{RR} + \frac{\alpha^{||}\tau_{ee}}{\tau_{ei}}\right)\frac{u_{e0z}}{v_{te}} + \frac{8i}{3}\bar{K}_{RS}, \tag{B17}$$

$$\bar{c}_{C||}^\perp = \frac{2}{3}\bar{c}_{Q||} - \frac{2}{5}\bar{k}_{||}\bar{K}_{hS} - \frac{1}{3}\bar{k}_{||}\bar{K}_{\sigma S} + \frac{2.05 - \bar{K}_{SS}}{3}, \tag{B18}$$

$$\bar{c}_{C\perp}^\perp = \frac{2}{3}\bar{c}_{Q\perp} - \frac{4}{15}\bar{k}_{||}\bar{K}_{hS} + \frac{1}{3}\bar{k}_{||}\bar{K}_{\sigma S} - \frac{2.05 - \bar{K}_{SS}}{3}, \tag{B19}$$

$$\bar{c}_{Cu}^\perp = \frac{4}{3}\left(1 - \bar{K}_{RR} + \frac{\alpha^{||}\tau_{ee}}{\tau_{ei}}\right)\frac{u_{e0z}}{v_{te}} - \frac{4i}{3}\bar{K}_{RS}. \tag{B20}$$

With these closures, Eqs. (20) and (21) can be written as

$$ir\alpha_e T_{e1}^{\|} = \bar{c}_{\|}^{\|} T_{e1}^{\|} + \bar{c}_{\perp}^{\|} T_{e1}^{\perp} + \bar{c}_{u}^{\|} T_{e0}\frac{u_{e1z}}{v_{te}} - \bar{c}_{ux} T_{e0}\frac{u_{e1x}}{v_{te}} - \bar{c}_n T_{e0}\frac{n_{e1}}{n_0} + A_t^{\|}, \tag{B21}$$

$$ir\alpha_e T_{e1}^{\perp} = \bar{c}_{\|}^{\perp} T_{e1}^{\|} + \bar{c}_{\perp}^{\perp} T_{e1}^{\perp} + \bar{c}_{u}^{\perp} T_{e0}\frac{u_{e1z}}{v_{te}} + (i\bar{k}_{\perp} - \bar{c}_{ux}) T_{e0}\frac{u_{e1x}}{v_{te}} - \bar{c}_n T_{e0}\frac{n_{e1}}{n_0} + A_t^{\perp}, \tag{B22}$$

where

$$\alpha_e = (\omega - \mathbf{k}\cdot\mathbf{u}_{e0})/\omega_{ce}, \tag{B23}$$

$$\bar{c}_{\|}^{\|} = \bar{k}_{\|}\bar{c}_{q\|}^{\|} - \bar{c}_{C\|}^{\|} + ir_{te}k_{\perp}\tau_{ee}u_{e0x}, \tag{B24}$$

$$\bar{c}_{\perp}^{\|} = \bar{k}_{\|}\bar{c}_{q\perp}^{\|} - \bar{c}_{C\perp}^{\|} - ir_{te}k_{\perp}\tau_{ee}u_{e0x}, \tag{B25}$$

$$\bar{c}_{u}^{\|} = i\bar{k}_{\|}\bar{c}_{qu}^{\|} - \bar{c}_{Cu}^{\|} + 2i\bar{k}_{\|}, \tag{B26}$$

$$\bar{c}_{ux} = \frac{8\alpha^{\perp}\tau_{ee}u_{e0x}}{3\tau_{ei}v_{te}}, \tag{B27}$$

$$\bar{c}_n = \frac{2m_e\tau_{ee}}{m_i\tau_{ei}}\left(\frac{T_{i0}}{T_{e0}} - 1\right) + \frac{4\alpha^{\perp}\tau_{ee}u_{e0x}^2}{3\tau_{ei}v_{te}^2}, \tag{B28}$$

$$\bar{c}_{\|}^{\perp} = \bar{k}_{\|}\bar{c}_{q\|}^{\perp} - \bar{c}_{C\|}^{\perp} - ir_{te}k_{\perp}\tau_{ee}u_{e0x}, \tag{B29}$$

$$\bar{c}_{\perp}^{\perp} = \bar{k}_{\|}\bar{c}_{q\perp}^{\perp} - \bar{c}_{C\perp}^{\perp} + ir_{te}k_{\perp}\tau_{ee}u_{e0x}, \tag{B30}$$

$$\bar{c}_{u}^{\perp} = i\bar{k}_{\|}\bar{c}_{qu}^{\perp} - \bar{c}_{Cu}^{\perp}, \tag{B31}$$

$$A_t^{\|} = -\frac{2m_e\tau_{ee}}{m_i\tau_{ei}}T_{i1} - \left(i\bar{k}_{\|}\bar{c}_{qu}^{\|} - \bar{c}_{Cu}^{\|}\right)T_{e0}\frac{u_{i1z}}{v_{te}} + \frac{8\alpha^{\perp}\tau_{ee}u_{e0x}}{3\tau_{ei}v_{te}}T_{e0}\frac{u_{i1x}}{v_{te}}, \tag{B32}$$

$$A_t^{\perp} = -\frac{2m_e\tau_{ee}}{m_i\tau_{ei}}T_{i1} - \left(i\bar{k}_{\|}\bar{c}_{qu}^{\perp} - \bar{c}_{Cu}^{\perp}\right)T_{e0}\frac{u_{i1z}}{v_{te}} + \frac{8\alpha^{\perp}\tau_{ee}u_{e0x}}{3\tau_{ei}v_{te}}T_{e0}\frac{u_{i1x}}{v_{te}}. \tag{B33}$$

With Eqs. (B21) and (B22), $T_{e1}^{\|}$ and $T_{e1}^{\perp}$ can be written as

$$T_{e1}^{\|} = \bar{c}_{uz}^{\|}T_{e0}\frac{u_{e1z}}{v_{te}} + \bar{c}_{ux}^{\|}T_{e0}\frac{u_{e1x}}{v_{te}} + \bar{c}_{n}^{\|}T_{e0}\frac{n_{e1}}{n_0} + A_i^{\|}, \tag{B34}$$

$$T_{e1}^{\perp} = \bar{c}_{uz}^{\perp}T_{e0}\frac{u_{e1z}}{v_{te}} + \bar{c}_{ux}^{\perp}T_{e0}\frac{u_{e1x}}{v_{te}} + \bar{c}_{n}^{\perp}T_{e0}\frac{n_{e1}}{n_0} + A_i^{\perp}, \tag{B35}$$

where

$$\bar{c}_{uz}^{\|} = \frac{(ir\alpha_e - \bar{c}_{\perp}^{\perp})\bar{c}_u^{\|} + \bar{c}_{\perp}^{\|}\bar{c}_u^{\perp}}{\left(ir\alpha_e - \bar{c}_{\|}^{\|}\right)\left(ir\alpha_e - \bar{c}_{\perp}^{\perp}\right) - \bar{c}_{\perp}^{\|}\bar{c}_{\|}^{\perp}}, \tag{B36}$$

$$\bar{c}_{ux}^{\|} = -\frac{(ir\alpha_e - \bar{c}_{\perp}^{\perp})\bar{c}_{ux} - \bar{c}_{\perp}^{\|}(i\bar{k}_{\perp} - \bar{c}_{ux})}{\left(ir\alpha_e - \bar{c}_{\|}^{\|}\right)\left(ir\alpha_e - \bar{c}_{\perp}^{\perp}\right) - \bar{c}_{\perp}^{\|}\bar{c}_{\|}^{\perp}}, \tag{B37}$$

$$\bar{c}_{n}^{\|} = -\frac{\left(ir\alpha_e - \bar{c}_{\perp}^{\perp} + \bar{c}_{\perp}^{\|}\right)\bar{c}_n}{\left(ir\alpha_e - \bar{c}_{\|}^{\|}\right)\left(ir\alpha_e - \bar{c}_{\perp}^{\perp}\right) - \bar{c}_{\perp}^{\|}\bar{c}_{\|}^{\perp}}, \tag{B38}$$

$$\bar{c}_{uz}^{\perp} = \frac{\left(ir\alpha_e - \bar{c}_{\|}^{\|}\right)\bar{c}_u^{\perp} + \bar{c}_{\|}^{\perp}\bar{c}_u^{\|}}{\left(ir\alpha_e - \bar{c}_{\|}^{\|}\right)\left(ir\alpha_e - \bar{c}_{\perp}^{\perp}\right) - \bar{c}_{\perp}^{\|}\bar{c}_{\|}^{\perp}}, \tag{B39}$$

$$\bar{c}_{ux}^{\perp} = \frac{\left(ir\alpha_e - \bar{c}_{\|}^{\|}\right)\left(i\bar{k}_{\perp} - \bar{c}_{ux}\right) - \bar{c}_{\|}^{\perp}\bar{c}_{ux}}{\left(ir\alpha_e - \bar{c}_{\|}^{\|}\right)\left(ir\alpha_e - \bar{c}_{\perp}^{\perp}\right) - \bar{c}_{\perp}^{\|}\bar{c}_{\|}^{\perp}}, \tag{B40}$$

$$\bar{c}_{n}^{\perp} = -\frac{\left(ir\alpha_e - \bar{c}_{\|}^{\|} + \bar{c}_{\|}^{\perp}\right)\bar{c}_n}{\left(ir\alpha_e - \bar{c}_{\|}^{\|}\right)\left(ir\alpha_e - \bar{c}_{\perp}^{\perp}\right) - \bar{c}_{\perp}^{\|}\bar{c}_{\|}^{\perp}}. \tag{B41}$$

The additional ion terms $A_i^{\|}$ and $A_i^{\perp}$ can be expressed as

$$A_i^{\|} = \bar{c}_{i\|}^{\|}A_t^{\|} + \bar{c}_{i\perp}^{\|}A_t^{\perp}, \tag{B42}$$

$$A_i^{\perp} = \bar{c}_{i\|}^{\perp}A_t^{\|} + \bar{c}_{i\perp}^{\perp}A_t^{\perp}, \tag{B43}$$

where

$$\bar{c}_{i\|}^{\|} = \frac{ir\alpha_e - \bar{c}_{\perp}^{\perp}}{\left(ir\alpha_e - \bar{c}_{\|}^{\|}\right)\left(ir\alpha_e - \bar{c}_{\perp}^{\perp}\right) - \bar{c}_{\perp}^{\|}\bar{c}_{\|}^{\perp}}, \tag{B44}$$

$$\bar{c}_{i\perp}^{\|} = \frac{\bar{c}_{\perp}^{\|}}{\left(ir\alpha_e - \bar{c}_{\|}^{\|}\right)\left(ir\alpha_e - \bar{c}_{\perp}^{\perp}\right) - \bar{c}_{\perp}^{\|}\bar{c}_{\|}^{\perp}}, \tag{B45}$$

$$\bar{c}_{i\|}^{\perp} = \frac{\bar{c}_{\|}^{\perp}}{\left(ir\alpha_e - \bar{c}_{\|}^{\|}\right)\left(ir\alpha_e - \bar{c}_{\perp}^{\perp}\right) - \bar{c}_{\perp}^{\|}\bar{c}_{\|}^{\perp}}, \tag{B46}$$

$$\bar{c}_{i\perp}^{\perp} = \frac{ir\alpha_e - \bar{c}_{\|}^{\|}}{\left(ir\alpha_e - \bar{c}_{\|}^{\|}\right)\left(ir\alpha_e - \bar{c}_{\perp}^{\perp}\right) - \bar{c}_{\perp}^{\|}\bar{c}_{\|}^{\perp}}. \tag{B47}$$

The z component of Eq. (8) is

$$im_e n_0(\omega - \mathbf{k}\cdot\mathbf{u}_0)u_{e1z} = ik_{\|}p_{e1}^{\|} + en_0(E_{1z} + u_{0x}B_{1y}) - R_{e1}^{\|}. \tag{B48}$$

From the Faraday's Law ($\omega\mathbf{B}_1 = \mathbf{k}\times\mathbf{E}_1$), $B_{1y} = (k_{\|}E_{1x} - k_{\perp}E_{1z})/\omega$. With Eqs. (9), (42), (B34), (B35), and (B48), u_{e1z} is expressed as

$$i\alpha_{ez}u_{e1z} = i\bar{c}_{xz}u_{e1x} + \bar{c}_{yz}u_{e1y} + A_{ez} + A_{iz}, \tag{B49}$$

where

$$\alpha_{ez} = \alpha_e - \frac{k_{\|}v_{te}}{2\omega_{ce}}\left[\bar{c}_{uz}^{\|} + \gamma_{ez}^{\|}\bar{c}_{uz}^{\|} + \gamma_{ez}^{\perp}\bar{c}_{uz}^{\perp} - \frac{2i(1-\bar{K}_{RR})}{\bar{k}_{\|}} + \frac{k_{\|}v_{te}}{\alpha_e\omega_{ce}}\left(1 + \bar{c}_n^{\|} + \gamma_{ez}^{\|}\bar{c}_n^{\|} + \gamma_{ez}^{\perp}\bar{c}_n^{\perp}\right)\right], \tag{B50}$$

$$\bar{c}_{xz} = \frac{k_{\|}v_{te}}{2\omega_{ce}}\left[\bar{c}_{ux}^{\|} + \gamma_{ez}^{\|}\bar{c}_{ux}^{\|} + \gamma_{ez}^{\perp}\bar{c}_{ux}^{\perp} + \frac{k_{\perp}v_{te}}{\alpha_e\omega_{ce}}\left(1 + \bar{c}_n^{\|} + \gamma_{ez}^{\|}\bar{c}_n^{\|} + \gamma_{ez}^{\perp}\bar{c}_n^{\perp}\right)\right], \tag{B51}$$

$$\bar{c}_{yz} = \frac{\varepsilon k_{\|}v_{te}^2}{2\alpha_e\omega_{ce}^2}\left(1 + \bar{c}_n^{\|} + \gamma_{ez}^{\|}\bar{c}_n^{\|} + \gamma_{ez}^{\perp}\bar{c}_n^{\perp}\right), \tag{B52}$$

$$A_{ez} = \frac{E_{1z}}{B_0} + \frac{ku_{0x}}{\omega}\frac{E_{1x}\cos\theta - E_{1z}\sin\theta}{B_0}, \tag{B53}$$

$$A_{iz} = \frac{ik_{\|}}{eB_0}\left(A_i^{\|} + \gamma_{ez}^{\|}A_i^{\|} + \gamma_{ez}^{\perp}A_i^{\perp}\right) - \frac{1 - \bar{K}_{RR}}{\omega_{ce}\tau_{ee}}u_{i1z}. \tag{B54}$$

The x component of Eq. (8) is

$$im_e n_0(\omega - \mathbf{k}\cdot\mathbf{u}_{e0})u_{e1x} = ik_{\perp}(n_0T_{e1}^{\perp} + T_{e0}n_{e1}) + en_0(E_{1x} + B_0u_{e1y} - u_{e0z}B_{1y}) - R_{e1}^{\perp}. \tag{B55}$$

With Eqs. (9), (45), (B34), (B35), (B49), and (B55), u_{e1y} can be expressed as

$$\gamma_{ey} u_{e1y} = i\alpha_{ex} u_{e1x} - A_{ex} - A_{ix} - \frac{\bar{c}_{zx} k_\perp v_{te}}{2\alpha_{ez}\omega_{ce}}(A_{ez} + A_{iz}), \tag{B56}$$

where γ_{ey}, α_{ex}, and A_{ex} are

$$\gamma_{ey} = 1 + \frac{\bar{c}_{nx}\varepsilon k_\perp v_{te}^2}{2\alpha_e \omega_{ce}^2} + \frac{\bar{c}_{zx}\bar{c}_{yz} k_\perp v_{te}}{2\alpha_{ez}\omega_{ce}}, \tag{B57}$$

$$\alpha_{ex} = \alpha_e - \frac{\bar{c}_{nx} k_\perp^2 v_{te}^2}{2\alpha_e \omega_{ce}^2} - \frac{\bar{c}_{zx}\bar{c}_{xz} k_\perp v_{te}}{2\alpha_{ez}\omega_{ce}} - \frac{k_\perp v_{te}}{2\omega_{ce}}\left[\frac{\beta^\perp \bar{c}_{ux}^{\|}}{3} + \left(1 + \frac{2\beta^\perp}{3}\right)\bar{c}_{ux}^{\perp} - \frac{2i\alpha^\perp \tau_{ee}}{k_\perp \tau_{ei}}\right], \tag{B58}$$

$$A_{ex} = \frac{E_{1x}}{B_0} - \frac{k u_{0z}}{\omega}\frac{E_{1x}\cos\theta - E_{1z}\sin\theta}{B_0}, \tag{B59}$$

$$A_{ix} = \frac{ik_\perp}{eB_0}\left[\frac{\beta^\perp A_i^{\|}}{3} + \left(1 + \frac{2\beta^\perp}{3}\right)A_i^\perp\right] - \frac{\alpha^\perp u_{i1x}}{\tau_{ei}\omega_{ce}}. \tag{B60}$$

Here, two dimensionless parameters are given by

$$\bar{c}_{nx} = 1 + \frac{\beta^\perp \bar{c}_n^{\|}}{3} + \left(1 + \frac{2\beta^\perp}{3}\right)\bar{c}_n^\perp - \frac{2i\alpha^\perp \tau_{ee} u_{e0x}}{k_\perp \tau_{ei} v_{te}}, \tag{B61}$$

$$\bar{c}_{zx} = \frac{\beta^\perp \bar{c}_{uz}^{\|}}{3} + \left(1 + \frac{2\beta^\perp}{3}\right)\bar{c}_{uz}^\perp + \frac{\bar{c}_{nx} k_\| v_{te}}{\alpha_e \omega_{ce}}. \tag{B62}$$

Similarly, the y component of Eq. (8) is

$$im_e n_0(\omega - \mathbf{k}\cdot\mathbf{u}_0)u_{e1y} = en_0(E_{1y} - B_0 u_{e1x} - u_{e0x}B_{1z} + u_{e0z}B_{1x}) + e(E_0 - u_{e0x}B_0)n_{e1} - R_{e1}^\times. \tag{B63}$$

With Eqs. (3), (9), and (B49), u_{e1x} can be expressed as

$$\gamma_{ex} u_{e1x} = -i\alpha_{ey} u_{e1y} + \frac{3ir_{te} k_\| u_{0x}}{2\alpha_e \alpha_{ez}\omega_{ce}}(A_{ez} + A_{iz}) + A_{ey} + A_{iy}, \tag{B64}$$

where γ_{ex}, α_{ey}, A_{ey}, and A_{iy} are

$$\gamma_{ex} = 1 + \frac{3r_{te} k_\perp u_{e0x}}{2\alpha_e \omega_{ce}}\left(1 + \frac{\bar{c}_{xz} k_\|}{\alpha_{ez} k_\perp}\right), \tag{B65}$$

$$\alpha_{ey} = \alpha_e - i\frac{\alpha^\times}{\omega_{ce}\tau_{ei}} - \frac{3r_{te}\varepsilon u_{e0x}}{2\alpha_e \omega_{ce}}\left(1 + \frac{\bar{c}_{yz} k_\|}{\alpha_{ez}\varepsilon}\right), \tag{B66}$$

$$A_{ey} = \frac{E_{1y}}{B_0} - \frac{k}{\omega}\frac{(u_{0x}\sin\theta + u_{0z}\cos\theta)E_{1y}}{B_0}, \tag{B67}$$

$$A_{iy} = \frac{\alpha^\times}{\omega_{ce}\tau_{ei}} u_{i1y}. \tag{B68}$$

With Eqs. (B56) and (B64), u_{e1y} is given by

$$u_{e1y} = i\left[iC_{yx}^e(A_{ex} + A_{ix}) + C_{yy}^e(A_{ey} + A_{iy}) + iC_{yz}^e(A_{ez} + A_{iz})\right], \tag{B69}$$

where

$$C_{yx}^e = \left(\gamma_{ey} - \frac{\alpha_{ex}\alpha_{ey}}{\gamma_{ex}}\right)^{-1}, \tag{B70}$$

$$C_{yy}^e = C_{yx}^e \frac{\alpha_{ex}}{\gamma_{ex}}, \tag{B71}$$

$$C_{yz}^e = C_{yx}^e\left(\frac{\bar{c}_{zx} k_\perp v_{te}}{2\alpha_{ez}\omega_{ce}} + \frac{3r_{te}\alpha_{ex} k_\| u_{e0x}}{2\gamma_{ex}\alpha_e \alpha_{ez}\omega_{ce}}\right). \tag{B72}$$

Similarly, u_{e1x} is given by

$$u_{e1x} = iC_{xx}^e(A_{ex} + A_{ix}) + C_{xy}^e(A_{ey} + A_{iy}) + iC_{xz}^e(A_{ez} + A_{iz}), \tag{B73}$$

where

$$C_{xy}^e = \left(\gamma_{ex} - \frac{\alpha_{ex}\alpha_{ey}}{\gamma_{ey}}\right)^{-1}, \tag{B74}$$

$$C_{xx}^e = C_{xy}^e \frac{\alpha_{ey}}{\gamma_{ey}}, \tag{B75}$$

$$C_{xz}^e = C_{xy}^e\left[\frac{3r_{te} k_\| u_{0x}}{2\alpha_e \alpha_{ez}\omega_{ce}} + \frac{\alpha_{ey}\bar{c}_{zx} k_\perp v_{te}}{2\gamma_{ey}\alpha_{ez}\omega_{ce}}\right]. \tag{B76}$$

Then, u_{e1z} can be written as

$$u_{e1z} = iC_{zx}^e(A_{ex} + A_{ix}) + C_{zy}^e(A_{ey} + A_{iy}) + iC_{zz}^e(A_{ez} + A_{iz}), \tag{B77}$$

where

$$C_{zz}^e = -\frac{1}{\alpha_{ez}} + \frac{\bar{c}_{xz}C_{xz}^e}{\alpha_{ez}} + \frac{\bar{c}_{yz}C_{yz}^e}{\alpha_{ez}}, \tag{B78}$$

$$C_{zx}^e = \frac{\bar{c}_{xz}C_{xx}^e}{\alpha_{ez}} + \frac{\bar{c}_{yz}C_{yx}^e}{\alpha_{ez}}, \tag{B79}$$

$$C_{zy}^e = \frac{\bar{c}_{xz}C_{xy}^e}{\alpha_{ez}} + \frac{\bar{c}_{yz}C_{yy}^e}{\alpha_{ez}}. \tag{B80}$$

The final goal is to obtain the perturbed current density of electrons, which is given by $\mathbf{J}_1^e = -en_0\mathbf{u}_{e1} - e\mathbf{u}_{e0}n_{e1}$. Thus, an expression for n_{e1} is required. From Eqs. (9), (B69), (B73), and (B77), n_{e1} is given by

$$n_{e1} = \frac{kn_0}{\omega - \mathbf{k}\cdot\mathbf{u}_{e0}}\left[iC_x'^e(A_{ex} + A_{ix}) + C_y'^e(A_{ey} + A_{iy}) + iC_z'^e(A_{ez} + A_{iz})\right], \tag{B81}$$

where

$$C_x'^e = C_{xx}^e\sin\theta + C_{yx}^e\varepsilon/k + C_{zx}^e\cos\theta, \tag{B82}$$

$$C_y'^e = C_{xy}^e\sin\theta + C_{yy}^e\varepsilon/k + C_{zy}^e\cos\theta, \tag{B83}$$

$$C_z'^e = C_{xz}^e\sin\theta + C_{yz}^e\varepsilon/k + C_{zz}^e\cos\theta. \tag{B84}$$

Now, we are ready for computing the dispersion relation. Equation (5) is

$$k_\|^2 E_{1x} - k_\perp k_\| E_{1z} - i\omega\mu_0 J_{1x} = 0, \tag{B85}$$

$$k^2 E_{1y} - i\omega\mu_0 J_{1y} = 0, \tag{B86}$$

$$k_\perp^2 E_{1z} - k_\perp k_\| E_{1x} - i\omega\mu_0 J_{1z} = 0. \tag{B87}$$

By multiplying by d_i^2 ($d_i \equiv c/\omega_{pi}$ is the ion skin depth; ω_{pi} is ion plasma frequency), the above equation can be written as

$$K^2\cos^2\theta E_{1x} - K^2\sin\theta\cos\theta E_{1z} - i\Omega\frac{B_0}{en_0}J_{1x} = 0, \tag{B88}$$

$$K^2 E_{1y} - i\Omega\frac{B_0}{en_0}J_{1y} = 0, \tag{B89}$$

$$K^2\sin^2\theta E_{1z} - K^2\sin\theta\cos\theta E_{1x} - i\Omega\frac{B_0}{en_0}J_{1z} = 0, \tag{B90}$$

where $K \equiv kd_{\rm i}$ and $\Omega = \omega/\omega_{\rm ci}$.

From Eq. (6), each component of $i\Omega B_0 \mathbf{J}_1^{\rm i}/en_0$ is

$$\frac{i\Omega B_0}{en_0}J_{1x}^{\rm i} = \zeta Z E_{1x} + \frac{\zeta Z''\sin\theta}{2}\left(E_{1x}\sin\theta - i\frac{\varepsilon}{k}E_{1y} + E_{1z}\cos\theta\right), \tag{B91}$$

$$\frac{i\Omega B_0}{en_0}J_{1y}^{\rm i} = \zeta Z E_{1y}, \tag{B92}$$

$$\frac{i\Omega B_0}{en_0}J_{1z}^{\rm i} = \zeta Z E_{1z} + \frac{\zeta Z''\cos\theta}{2}\left(E_{1x}\sin\theta - i\frac{\varepsilon}{k}E_{1y} + E_{1z}\cos\theta\right). \tag{B93}$$

From Eqs. (B73) and (B81), $iJ_{1x}^{\rm e}/en_0$ is given by

$$\frac{iJ_{1x}^{\rm e}}{en_0} = C_{xx}^{\rm e\prime}(A_{\rm ex}+A_{\rm ix}) - iC_{xy}^{\rm e\prime}(A_{\rm ey}+A_{\rm iy}) + C_{xz}^{\rm e\prime}(A_{\rm ez}+A_{\rm iz}), \tag{B94}$$

where $C_{xx}^{\rm e\prime} = C_{xx}^{\rm e} + ku_{\rm e0x}C_x^{\prime\rm e}/(\omega - \mathbf{k}\cdot\mathbf{u}_{\rm e0})$, $C_{xy}^{\rm e\prime} = C_{xy}^{\rm e} + ku_{\rm e0x}C_y^{\prime\rm e}/(\omega - \mathbf{k}\cdot\mathbf{u}_{\rm e0})$, and $C_{xz}^{\rm e\prime} = C_{xz}^{\rm e} + ku_{\rm e0x}C_z^{\prime\rm e}/(\omega - \mathbf{k}\cdot\mathbf{u}_{\rm e0})$. Similarly, from Eqs. (B77) and (B81), $iJ_{1z}^{\rm e}/en_0$ is given by

$$\frac{iJ_{1z}^{\rm e}}{en_0} = C_{zx}^{\rm e\prime}(A_{\rm ex}+A_{\rm ix}) - iC_{zy}^{\rm e\prime}(A_{\rm ey}+A_{\rm iy}) + C_{zz}^{\rm e\prime}(A_{\rm ez}+A_{\rm iz}), \tag{B95}$$

where $C_{zx}^{\rm e\prime} = C_{zx}^{\rm e} + ku_{\rm e0z}C_x^{\prime\rm e}/(\omega - \mathbf{k}\cdot\mathbf{u}_{\rm e0})$, $C_{zy}^{\rm e\prime} = C_{zy}^{\rm e} + ku_{\rm e0z}C_y^{\prime\rm e}/(\omega - \mathbf{k}\cdot\mathbf{u}_{\rm e0})$, and $C_{zz}^{\rm e\prime} = C_{zz}^{\rm e} + ku_{\rm e0z}C_z^{\prime\rm e}/(\omega - \mathbf{k}\cdot\mathbf{u}_{\rm e0})$. Since there is no y component in $\mathbf{u}_{\rm e0}$, $iJ_{1y}^{\rm e}/en_0$ is simply

$$\frac{iJ_{1y}^{\rm e}}{en_0} = iC_{yx}^{\rm e}(A_{\rm ex}+A_{\rm ix}) + C_{yy}^{\rm e}(A_{\rm ey}+A_{\rm iy}) + iC_{yz}^{\rm e}(A_{\rm ez}+A_{\rm iz}). \tag{B96}$$

In terms of dimensionless parameters, $\Omega B_0 A_{\rm ex}$, $\Omega B_0 A_{\rm ey}$, and $\Omega B_0 A_{\rm ez}$ can be written as

$$\Omega B_0 A_{\rm ex} = (\Omega - KU_{\rm e0z}\cos\theta)E_{1x} + (KU_{\rm e0z}\sin\theta)E_{1z}, \tag{B97}$$

$$\Omega B_0 A_{\rm ey} = [\Omega - K(U_{\rm e0x}\sin\theta + U_{\rm e0z}\cos\theta)]E_{1y}, \tag{B98}$$

$$\Omega B_0 A_{\rm ez} = (KU_{\rm e0x}\cos\theta)E_{1x} + (\Omega - KU_{\rm e0x}\sin\theta)E_{1z}. \tag{B99}$$

$\mathbf{U}_{\rm e0} = \mathbf{u}_{\rm e0}/V_{\rm A}$ and $V_{\rm A} = B_0/\sqrt{\mu_0 m_{\rm i} n_0} = d_{\rm i}\omega_{\rm ci}$ is the Alfvén speed.

With Eq. (7), $A_{\rm iz}$ in Eq. (B54) is

$$A_{\rm iz} = \bar{c}_{{\rm i}zx}\frac{iJ_{1x}^{\rm i}}{en_0} + \bar{c}_{{\rm i}zz}\frac{iJ_{1z}^{\rm i}}{en_0} + \frac{\bar{c}_{{\rm i}zT}}{B_0}\left[\mathbf{E}_1\cdot\hat{\mathbf{k}}\left(2Z' + \frac{Z'''}{4}\right) - iE_{1y}\left(\frac{\varepsilon}{k}\right)\left(Z' + \frac{Z'''}{4}\right)\right], \tag{B100}$$

where three dimensionless parameters are given by

$$\bar{c}_{{\rm i}zx} = \frac{4\alpha^{\perp}(\bar{c}_{\rm iz}^{||} + \bar{c}_{\rm iz}^{\perp})\tau_{\rm ee}k_{||}u_{\rm e0x}}{3\tau_{\rm ei}\omega_{\rm ce}}, \tag{B101}$$

$$\bar{c}_{{\rm i}zz} = -\left[\bar{c}_{\rm iz}^{||}\left(i\bar{k}_{||}\bar{c}_{qu}^{||} - \bar{c}_{Cu}^{||}\right) + \bar{c}_{\rm iz}^{\perp}\left(i\bar{k}_{||}\bar{c}_{qu}^{\perp} - \bar{c}_{Cu}^{\perp}\right)\right]\frac{k_{||}v_{\rm te}}{2\omega_{\rm ce}} + \frac{i(1-\bar{K}_{RR})}{\omega_{\rm ce}\tau_{\rm ee}}, \tag{B102}$$

$$\bar{c}_{{\rm i}zT} = \frac{2(\bar{c}_{\rm iz}^{||} + \bar{c}_{\rm iz}^{\perp})m_{\rm e}\tau_{\rm ee}\cos\theta}{m_{\rm i}\tau_{\rm ei}}. \tag{B103}$$

Here, two additional parameters $\bar{c}_{\rm iz}^{||}$ and $\bar{c}_{\rm iz}^{\perp}$ are defined as

$$\bar{c}_{\rm iz}^{||} = (1+\gamma_{\rm ez}^{||})\bar{c}_{\rm i||}^{||} + \gamma_{\rm ez}^{\perp}\bar{c}_{\rm i||}^{\perp}, \tag{B104}$$

$$\bar{c}_{\rm iz}^{\perp} = (1+\gamma_{\rm ez}^{||})\bar{c}_{\rm i\perp}^{||} + \gamma_{\rm ez}^{\perp}\bar{c}_{\rm i\perp}^{\perp}. \tag{B105}$$

Similarly, $A_{\rm ix}$ is

$$A_{\rm ix} = \bar{c}_{{\rm i}xx}\frac{iJ_{1x}^{\rm i}}{en_0} + \bar{c}_{{\rm i}xz}\frac{iJ_{1z}^{\rm i}}{en_0} + \frac{\bar{c}_{{\rm i}xT}}{B_0}\left[\mathbf{E}_1\cdot\hat{\mathbf{k}}\left(2Z' + \frac{Z'''}{4}\right) - iE_{1y}\left(\frac{\varepsilon}{k}\right)\left(Z' + \frac{Z'''}{4}\right)\right], \tag{B106}$$

where three dimensionless parameters are given by

$$\bar{c}_{{\rm i}xx} = \frac{4\alpha^{\perp}(\bar{c}_{\rm ix}^{||} + \bar{c}_{\rm ix}^{\perp})\tau_{\rm ee}k_{\perp}u_{\rm e0x}}{3\tau_{\rm ei}\omega_{\rm ce}} - \frac{\alpha^{\perp}}{\tau_{\rm ee}\omega_{\rm ce}}, \tag{B107}$$

$$\bar{c}_{{\rm i}xz} = -\left[\bar{c}_{\rm ix}^{||}\left(i\bar{k}_{||}\bar{c}_{qu}^{||} - \bar{c}_{Cu}^{||}\right) + \bar{c}_{\rm ix}^{\perp}\left(i\bar{k}_{||}\bar{c}_{qu}^{\perp} - \bar{c}_{Cu}^{\perp}\right)\right]\frac{k_{\perp}v_{\rm te}}{2\omega_{\rm ce}}, \tag{B108}$$

$$\bar{c}_{{\rm i}xT} = \frac{2(\bar{c}_{\rm ix}^{||} + \bar{c}_{\rm ix}^{\perp})m_{\rm e}\tau_{\rm ee}\sin\theta}{m_{\rm i}\tau_{\rm ei}}. \tag{B109}$$

Two additional parameters $\bar{c}_{\rm ix}^{||}$ and $\bar{c}_{\rm ix}^{\perp}$ are

$$\bar{c}_{\rm ix}^{||} = \frac{\beta^{\perp}}{3}\bar{c}_{\rm i||}^{||} + \left(1 + \frac{2\beta^{\perp}}{3}\right)\bar{c}_{\rm i||}^{\perp}, \tag{B110}$$

$$\bar{c}_{\rm ix}^{\perp} = \frac{\beta^{\perp}}{3}\bar{c}_{\rm i\perp}^{||} + \left(1 + \frac{2\beta^{\perp}}{3}\right)\bar{c}_{\rm i\perp}^{\perp}. \tag{B111}$$

The last ion term is $A_{\rm iy} = (\alpha^{\times}/\omega_{\rm ce}\tau_{\rm ei})J_{1y}^{\rm i}/en_0$.

Equations (B88)–(B90) can be written as

$$\begin{pmatrix} D_{xx} & D_{xy} & D_{xz} \\ D_{yx} & D_{yy} & D_{yz} \\ D_{zx} & D_{zy} & D_{zz} \end{pmatrix}\begin{pmatrix} E_{1x} \\ E_{1y} \\ E_{1z} \end{pmatrix} = 0. \tag{B112}$$

Each component of the tensor $\mathbf{D}$ is

$$D_{xx} = K^2\cos^2\theta - C_{xx}^{\rm e\prime}(\Omega - KU_{\rm e0z}\cos\theta) - C_{xz}^{\rm e\prime}KU_{\rm e0x}\cos\theta - C_{xx}^{\rm i}\left(\zeta Z + \frac{\zeta Z''\sin^2\theta}{2}\right) - C_{xz}^{\rm i}\frac{\zeta Z''\cos\theta\sin\theta}{2} - C_{xT}^{\rm i}\Omega\sin\theta\left(2Z' + \frac{Z'''}{4}\right), \tag{B113}$$

$$D_{xy} = C_{xy}^{\rm e\prime}\frac{\alpha^{\times}}{\omega_{\rm ce}\tau_{\rm ei}}\zeta Z + iC_{xy}^{\rm e\prime}[\Omega - K(U_{\rm e0x}\sin\theta + U_{\rm e0z}\cos\theta)] + i\left(\frac{\varepsilon}{k}\right)C_{xx}^{\rm i}\frac{\zeta Z''\sin\theta}{2} + i\left(\frac{\varepsilon}{k}\right)C_{xz}^{\rm i}\frac{\zeta Z''\cos\theta}{2} + i\left(\frac{\varepsilon}{k}\right)C_{xT}^{\rm i}\left(Z' + \frac{Z'''}{4}\right), \tag{B114}$$

$$D_{xz} = -K^2\sin\theta\cos\theta - C_{xx}^{\rm e\prime}KU_{\rm e0z}\sin\theta - C_{xz}^{\rm e\prime}(\Omega - KU_{\rm e0x}\sin\theta) - C_{xx}^{\rm i}\frac{\zeta Z''}{2}\sin\theta\cos\theta - C_{xz}^{\rm i}\left(\zeta Z + \frac{\zeta Z''\cos^2\theta}{2}\right) - C_{xT}^{\rm i}\Omega\cos\theta\left(2Z' + \frac{Z'''}{4}\right), \tag{B115}$$

$$D_{yx} = -i\left[C^{e}_{yx}(\Omega - KU_{e0z}\cos\theta) + C^{e}_{yz}KU_{e0x}\cos\theta\right] - iC^{i}_{yx}\left(\zeta Z + \frac{\zeta Z''\sin^2\theta}{2}\right) - iC^{i}_{yz}\frac{\zeta Z''\cos\theta\sin\theta}{2} - iC^{i}_{yT}\Omega\sin\theta\left(2Z' + \frac{Z'''}{4}\right), \tag{B116}$$

$$D_{yy} = K^2 - \left(1 - \frac{iC^{e}_{yy}\alpha^{\times}}{\omega_{ce}\tau_{ei}}\right)\zeta Z - C^{e}_{yy}[\Omega - K(U_{e0x}\sin\theta + U_{e0z}\cos\theta)] - \left(\frac{\varepsilon}{k}\right)C^{i}_{yx}\frac{\zeta Z''\sin\theta}{2} - \left(\frac{\varepsilon}{k}\right)C^{i}_{yz}\frac{\zeta Z''\cos\theta}{2} - \left(\frac{\varepsilon}{k}\right)C^{i}_{yT}\Omega\left(Z' + \frac{Z'''}{4}\right), \tag{B117}$$

$$D_{yz} = -i\left[C^{e}_{yx}KU_{e0z}\sin\theta + C^{e}_{yz}(\Omega - KU_{e0x}\sin\theta)\right] - iC^{i}_{yx}\frac{\zeta Z''\sin\theta\cos\theta}{2} - iC^{i}_{yz}\left(\zeta Z + \frac{\zeta Z''\cos^2\theta}{2}\right) - iC^{i}_{yT}\Omega\cos\theta\left(2Z' + \frac{Z'''}{4}\right), \tag{B118}$$

$$D_{zx} = -K^2\sin\theta\cos\theta - C^{e\prime}_{zx}(\Omega - KU_{e0z}\cos\theta) - C^{e\prime}_{zz}KU_{e0x}\cos\theta - C^{i}_{zx}\left(\zeta Z + \frac{\zeta Z''\sin^2\theta}{2}\right) - C^{i}_{zz}\frac{\zeta Z''\cos\theta\sin\theta}{2} - C^{i}_{zT}\Omega\sin\theta\left(2Z' + \frac{Z'''}{4}\right), \tag{B119}$$

$$D_{zy} = C^{e\prime}_{zy}\frac{\alpha^{\times}}{\omega_{ce}\tau_{ei}}\zeta Z + iC^{e\prime}_{zy}[\Omega - K(U_{e0x}\sin\theta + U_{e0z}\cos\theta)] + i\left(\frac{\varepsilon}{k}\right)C^{i}_{zx}\frac{\zeta Z''\sin\theta}{2} + i\left(\frac{\varepsilon}{k}\right)C^{i}_{zz}\frac{\zeta Z''\cos\theta}{2} + i\left(\frac{\varepsilon}{k}\right)C^{i}_{zT}\Omega\left(Z' + \frac{Z'''}{4}\right), \tag{B120}$$

$$D_{zz} = K^2\sin^2\theta - C^{e\prime}_{zx}KU_{e0z}\sin\theta - C^{e\prime}_{zz}(\Omega - KU_{e0x}\sin\theta) - C^{i}_{zx}\frac{\zeta Z''}{2}\sin\theta\cos\theta - C^{i}_{zz}\left(\zeta Z + \frac{\zeta Z''\cos^2\theta}{2}\right) - C^{i}_{zT}\Omega\cos\theta\left(2Z' + \frac{Z'''}{4}\right), \tag{B121}$$

where

$$C^{i}_{xx} = 1 + C^{e\prime}_{xx}\bar{c}_{ixx} + C^{e\prime}_{xz}\bar{c}_{izx}, \tag{B122}$$

$$C^{i}_{xz} = C^{e\prime}_{xx}\bar{c}_{ixz} + C^{e\prime}_{xz}\bar{c}_{izz}, \tag{B123}$$

$$C^{i}_{xT} = C^{e\prime}_{xx}\bar{c}_{ixT} + C^{e\prime}_{xz}\bar{c}_{izT}, \tag{B124}$$

$$C^{i}_{yx} = C^{e}_{yx}\bar{c}_{ixx} + C^{e}_{yz}\bar{c}_{izx}, \tag{B125}$$

$$C^{i}_{yz} = C^{e}_{yx}\bar{c}_{ixz} + C^{e}_{yz}\bar{c}_{izz}, \tag{B126}$$

$$C^{i}_{yT} = C^{e}_{yx}\bar{c}_{ixT} + C^{e}_{yz}\bar{c}_{izT}, \tag{B127}$$

$$C^{i}_{zx} = C^{e\prime}_{zx}\bar{c}_{ixx} + C^{e\prime}_{zz}\bar{c}_{izx}, \tag{B128}$$

$$C^{i}_{zz} = 1 + C^{e\prime}_{zx}\bar{c}_{ixz} + C^{e\prime}_{zz}\bar{c}_{izz}, \tag{B129}$$

$$C^{i}_{zT} = C^{e\prime}_{zx}\bar{c}_{ixT} + C^{e\prime}_{zz}\bar{c}_{izT}. \tag{B130}$$

APPENDIX C: COMPARISON WITH CLASSICAL MODEL

Since the current model has been established independently, benchmarking with the classical model is desirable. Here, we used the well-known model by Davidson *et al.*[17] For this benchmarking, we set both $k_{||}$ and u_{e0z} to be zero as in the classical model.

As shown in Fig. 8, the results from both collisional (blue line) and collisionless (red line) models do not agree with results from the classical model (black line). In particular, our models expect an almost linear dispersion relation, but ω increases slowly for small $k\rho_e$ in the classical model. Another interesting difference is that the peak growth rate occurs around $k\rho_e \sim 0.6$ in our models, while it is around $k\rho_e \sim 1$ in the classical model. This discrepancy is not due to the choice of our heat flux closures; there is not much difference between our two models, which shows the insensitivity of the dispersion to $p^{\perp}_{e1}$. Moreover, the dispersion relation is independent of $p^{||}_{e1}$ when $k_{||} = 0$. We also have confirmed that this discrepancy is not due to the inclusion of the perturbed ion current density, which is ignored in the classical model.

We note that the basic set of equations used in the classical model by Davidson *et al.*[17] is different. The biggest difference is that Poisson's equation is used in the classical model, while we used Faraday's induction law. To understand the cause of this discrepancy, we have developed another model to calculate the dispersion relation. In this model, we follow the basic equations of the classical model, while using our results for the perturbed density and current density.

In our geometry, the first-order equations in Davidson *et al.*[17] can be written as

$$E_{1y} - \frac{i\mu_0\omega}{k^2(1-\Delta^2)}J_{1y} = 0, \tag{C1}$$

$$E_{1x} + \frac{ie}{\varepsilon_0 k}(n_{i1} - n_{e1}) = 0, \tag{C2}$$

where $\Delta = \omega/(ck)$, which is from the displacement current. This contribution is ignored, since the phase velocity of LHDWs is much smaller than the speed of light ($|\Delta^2| \ll 1$). We have confirmed that the dispersion relation is insensitive to the inclusion of Δ^2.

For J_{1y}, n_{i1}, and n_{e1}, we use the results from our models. The perturbed ion density is given by[24]

$$n_{i1} = i\frac{n_0 e}{m_i k^2 v_{ti}^2}Z'(kE_{1x} - i\varepsilon E_{1y}). \tag{C3}$$

For the perturbed electron density, we will use one from the collisionless model for simplicity, as there is not much difference between two models. We also assume that $T_{e0} = T_{i0}$. With $k_{||} = 0$ and $u_{e0z} = 0$, n_{e1} can be expressed as[7]

$$n_{e1} = \frac{kn_0}{(\omega - ku_{e0x})B_0}\left[iC^{n}_{x}E_{1x} + C^{n}_{y}\left(1 - \frac{ku_{e0x}}{\omega}\right)E_{1y}\right], \tag{C4}$$

where

$$C^{n}_{x} = \left(\alpha_e + \frac{\varepsilon}{k}\right)\left[1 - \alpha_e^2 + \frac{1}{2\alpha_e}\left(\frac{\varepsilon k v_{te}^2}{\omega_{ce}^2} + \frac{ku_{e0x}}{\omega_{ce}}\right) + \frac{1}{2}\left(\frac{k^2 v_{te}^2}{\omega_{ce}^2} + \frac{\varepsilon u_{e0x}}{\omega_{ce}}\right)\right]^{-1}, \tag{C5}$$

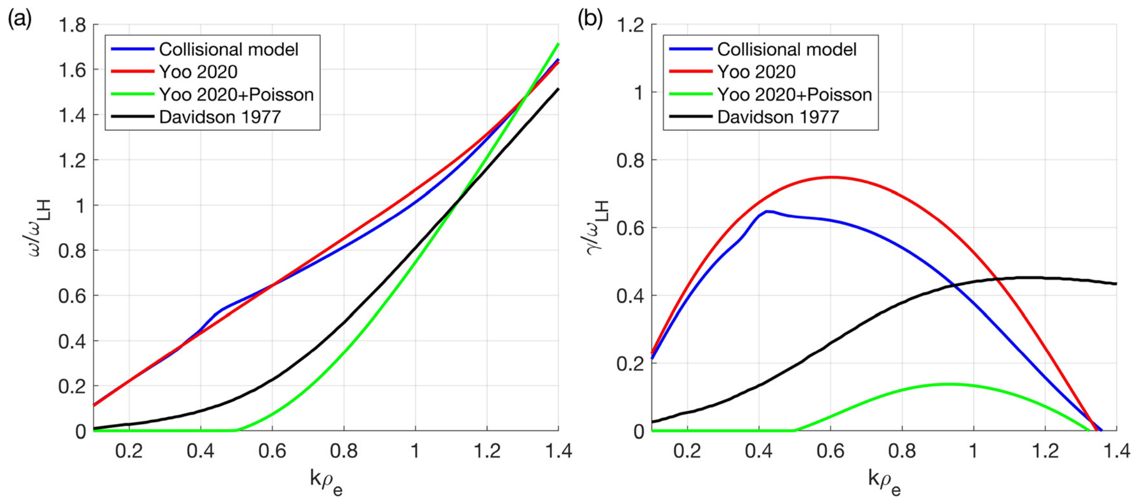

FIG. 8. Dispersion relation for the case of the ES-LHDW ($T_e = T_i = 10$ eV, $n_e = 2 \times 10^{13}$ cm^{-3}, $B_0 = 180$ Gauss, $u_{e0x} = 50$ km/s, singly ionized helium). (a) Dispersion relation for four cases. The blue and red lines indicate results from collisional and collisionless models, respectively. The green line denotes the case derived here with Poisson's equation and perturbed quantities in the collisionless model. The black lines indicate the results from the classical models.[17] (b) Growth rate of the ES-LHDW for all cases.

$$C_y^n = \left(1+\frac{\varepsilon}{k}\alpha_e\right)\left[1-\alpha_e^2+\frac{1}{2\alpha_e}\left(\frac{\varepsilon k v_{te}^2}{\omega_{ce}^2}+\frac{k u_{e0x}}{\omega_{ce}}\right)+\frac{1}{2}\left(\frac{k^2 v_{te}^2}{\omega_{ce}^2}+\frac{\varepsilon u_{e0x}}{\omega_{ce}}\right)\right]^{-1}. \tag{C6}$$

The y component of the perturbed ion current is[24]

$$J_{1y}^{i} = -\frac{ie^2 n_0}{m_i \omega}\zeta Z E_{1y}. \tag{C7}$$

The y component of the perturbed electron current is[7]

$$J_{1y}^{e} = -\frac{ien_0}{B_0}\left[iC_x^u E_{1x} + C_y^u\left(1-\frac{k u_{e0x}}{\omega}\right)E_{1y}\right], \tag{C8}$$

where

$$C_x^u = \left(1+\frac{k u_{e0x}}{2\alpha_e\omega_{ce}}\right)\left[1-\alpha_e^2+\frac{1}{2\alpha_e}\left(\frac{\varepsilon k v_{te}^2}{\omega_{ce}^2}+\frac{k u_{e0x}}{\omega_{ce}}\right) + \frac{1}{2}\left(\frac{k^2 v_{te}^2}{\omega_{ce}^2}+\frac{\varepsilon u_{e0x}}{\omega_{ce}}\right)\right]^{-1}, \tag{C9}$$

$$C_y^u = \left(\alpha_e-\frac{k^2 v_{te}^2}{2\alpha_e\omega_{ce}^2}\right)\left[1-\alpha_e^2+\frac{1}{2\alpha_e}\left(\frac{\varepsilon k v_{te}^2}{\omega_{ce}^2}+\frac{k u_{e0x}}{\omega_{ce}}\right) + \frac{1}{2}\left(\frac{k^2 v_{te}^2}{\omega_{ce}^2}+\frac{\varepsilon u_{e0x}}{\omega_{ce}}\right)\right]^{-1}. \tag{C10}$$

With Eqs. (C3), (C4), (C7), and (C8), Eqs. (C1) and (C2) can be written as

$$D_{yy}E_{1y} + D_{yx}E_{1x} = 0, \tag{C11}$$

$$D_{xy}E_{1y} + D_{xx}E_{1x} = 0, \tag{C12}$$

where

$$D_{yy} = 1 - \frac{\zeta Z}{K^2(1-\Delta^2)} - \frac{\Omega - KU_{e0x}}{K^2(1-\Delta^2)}C_y^u, \tag{C13}$$

$$D_{yx} = -\frac{i\Omega C_x^u}{K^2(1-\Delta^2)}, \tag{C14}$$

$$D_{xy} = \frac{id_i^2}{2K^2\lambda_{Di}^2}\left(\frac{\varepsilon}{k}\right)Z' - \frac{i\omega_{pi}^2 C_y^n}{\omega_{ci}^2\Omega}, \tag{C15}$$

$$D_{xx} = 1 - \frac{d_{i^2}}{2K^2\lambda_{Di}^2}Z' + \frac{\omega_{pi}^2 C_x^n}{\omega_{ci}^2(\Omega - KU_{e0x})}, \tag{C16}$$

where $\lambda_{Di} = \sqrt{\varepsilon_0 T_{i0}/e^2 n_0}$ is the ion Debye Length. The dispersion relation can be obtained by setting $D_{xx}D_{yy} - D_{xy}D_{yx} = 0$.

The dispersion relation from this simplified model (green line) agrees with the classical model, as shown in Fig. 8(a). This means that the discrepancy is due to the use of Poisson's equation, where the Faraday induction term is ignored. With the parameters for the ES-LHDW, β_e is about 0.25, which means that perturbed magnetic field due to the perturbed plasma current may not be negligible. This argument is supported by observations in laboratory and space,[7,10] where magnetic field fluctuations exist when there are strong electric field fluctuations associated with ES-LHDW.

It is interesting to see that the growth rate from the simplified model is considerably lower than that from the classical model, as shown in Fig. 8(b). This difference is likely related to the lack of a rigorous modeling of the heat flux in this simplified model. Although the magnitude is different, both models show that the peak growth rate is around $k\rho_e \sim 1$.

This comparison shows that the use of electron fluid equations is acceptable for dynamics of LHDWs. It should be also noted that only our models include full electromagnetic effects, since the induction term is included. These effects are important when β is not negligible.

REFERENCES

[1] S. D. Bale, F. S. Mozer, and T. Phan, "Observation of lower hybrid drift instability in the diffusion region at a reconnecting magnetopause," Geophys. Res. Lett. **29**, 33-1–33-4, https://doi.org/10.1029/2002GL016113 (2002).
[2] C. Norgren, A. Vaivads, Y. V. Khotyaintsev, and M. André, "Lower hybrid drift waves: Space observations," Phys. Rev. Lett. **109**, 055001 (2012).
[3] D. B. Graham, Y. V. Khotyaintsev, C. Norgren, A. Vaivads, M. André, S. Toledo-Redondo, P.-A. Lindqvist, G. T. Marklund, R. E. Ergun, W. R. Paterson, D. J. Gershman, B. L. Giles, C. J. Pollock, J. C. Dorelli, L. A. Avanov, B. Lavraud, Y. Saito, W. Magnes, C. T. Russell, R. J. Strangeway, R. B. Torbert, and J. L. Burch, "Lower hybrid waves in the ion diffusion and magnetospheric inflow regions," J. Geophys. Res. **122**, 517–533, https://doi.org/10.1002/2016JA023572 (2017).
[4] D. B. Graham, Y. V. Khotyaintsev, C. Norgren, A. Vaivads, M. André, J. F. Drake, J. Egedal, M. Zhou, O. L. Contel, J. M. Webster, B. Lavraud, I. Kacem, V. Génot, C. Jacquey, A. C. Rager, D. J. Gershman, J. L. Burch, and R. E. Ergun, "Universality of lower hybrid waves at Earth's magnetopause," J. Geophys. Res.: Space Phys. **124**, 8727–8760, https://doi.org/10.1029/2019JA027155 (2019).
[5] L.-J. Chen, S. Wang, M. Hesse, R. E. Ergun, T. Moore, B. Giles, N. Bessho, C. Russell, J. Burch, R. B. Torbert, K. J. Genestreti, W. Paterson, C. Pollock, B. Lavraud, O. L. Contel, R. Strangeway, Y. V. Khotyaintsev, and P.-A. Lindqvist, "Electron diffusion regions in magnetotail reconnection under varying guide fields," Geophys. Res. Lett. **46**, 6230–6238, https://doi.org/10.1029/2019GL082393 (2019).
[6] L.-J. Chen, S. Wang, O. L. Contel, A. Rager, M. Hesse, J. Drake, J. Dorelli, J. Ng, N. Bessho, D. Graham, L. B. Wilson, T. Moore, B. Giles, W. Paterson, B. Lavraud, K. Genestreti, R. Nakamura, Y. V. Khotyaintsev, R. E. Ergun, R. B. Torbert, J. Burch, C. Pollock, C. T. Russell, P.-A. Lindqvist, and L. Avanov, "Lower-hybrid drift waves driving electron nongyrotropic heating and vortical flows in a magnetic reconnection layer," Phys. Rev. Lett. **125**, 025103 (2020).
[7] J. Yoo, J.-Y. Ji, M. V. Ambat, S. Wang, H. Ji, J. Lo, B. Li, Y. Ren, J. Jara-Almonte, L.-J. Chen, W. Fox, M. Yamada, A. Alt, and A. Goodman, "Lower hybrid drift waves during guide field reconnection," Geophys. Res. Lett. **47**, e2020GL087192, https://doi.org/10.1029/2020GL087192 (2020).
[8] T. A. Carter, H. Ji, F. Trintchouk, M. Yamada, and R. M. Kulsrud, "Measurement of lower-hybrid drift turbulence in a reconnecting current sheet," Phys. Rev. Lett. **88**, 015001 (2001).
[9] H. Ji, S. Terry, M. Yamada, R. Kulsrud, A. Kuritsyn, and Y. Ren, "Electromagnetic fluctuations during fast reconnection in a laboratory plasma," Phys. Rev. Lett. **92**, 115001 (2004).
[10] J. Yoo, M. Yamada, H. Ji, J. Jara-Almonte, C. E. Myers, and L.-J. Chen, "Laboratory study of magnetic reconnection with a density asymmetry across the current sheet," Phys. Rev. Lett. **113**, 095002 (2014).
[11] P. H. Yoon and A. T. Y. Lui, "Lower-hybrid-drift and modified-two-stream instabilities in current sheet equilibrium," J. Geophys. Res. **109**, A02210, https://doi.org/10.1029/2003JA010180 (2004).
[12] R. Kulsrud, *Plasma Physics for Astrophysics* (Princeton University Press, Princeton, 2005).
[13] I. Silin, J. Büchner, and A. Vaivads, "Anomalous resistivity due to nonlinear lower-hybrid drift waves," Phys. Plasmas **12**, 062902 (2005).
[14] P. H. Yoon and A. T. Y. Lui, "Anomalous resistivity by fluctuation in the lower-hybrid frequency range," J. Geophys. Res.: Space Phys. **112**, A06207, https://doi.org/10.1029/2006JA012209 (2007).
[15] V. Roytershteyn, W. Daughton, H. Karimabadi, and F. S. Mozer, "Influence of the lower-hybrid drift instability on magnetic reconnection in asymmetric configurations," Phys. Rev. Lett. **108**, 185001 (2012).
[16] V. Roytershteyn, S. Dorfman, W. Daughton, H. Ji, M. Yamada, and H. Karimabadi, "Electromagnetic instability of thin reconnection layers: Comparison of three-dimensional simulations with MRX observations," Phys. Plasmas **20**, 061212 (2013).
[17] R. Davidson, N. Gladd, C. Wu, and J. Huba, "Effects of finite plasma beta on the lower-hybrid drift instability," Phys. Fluids **20**, 301 (1977).
[18] L. Spitzer, *Physics of Fully Ionized Gases*, 2nd ed. (Interscience Publishers, New York, 1962).
[19] A. Kuritsyn, M. Yamada, S. Gerhardt, H. Ji, R. Kulsrud, and Y. Ren, "Measurements of the parallel and transverse Spitzer resistivities during collisional magnetic reconnection," Phys. Plasmas **13**, 055703 (2006).
[20] J. Yoo, M. Yamada, H. Ji, J. Jara-Almonte, and C. E. Myers, "Bulk ion acceleration and particle heating during magnetic reconnection in a laboratory plasma," Phys. Plasmas **21**, 055706 (2014).
[21] W. Daughton, "Electromagnetic properties of the lower-hybrid drift instability in a thin current sheet," Phys. Plasmas **10**, 3103–3119 (2003).
[22] W. Daughton, G. Lapenta, and P. Ricci, "Nonlinear evolution of the lower-hybrid drift instability in a current sheet," Phys. Rev. Lett. **93**, 105004 (2004).
[23] X. Y. Wang, Y. Lin, L. Chen, and Z. Lin, "A particle simulation of current sheet instabilities under finite guide field," Phys. Plasmas **15**, 072103 (2008).
[24] H. Ji, R. Kulsrud, W. Fox, and M. Yamada, "An obliquely propagating electromagnetic drift instability in the lower hybrid frequency range," J. Geophys. Res. **110**, A08212, https://doi.org/10.1029/2005JA011188 (2005).
[25] J.-Y. Ji and I. Joseph, "Electron parallel closures for the 3 + 1 fluid model," Phys. Plasmas **25**, 032117 (2018).
[26] J.-Y. Ji and E. D. Held, "Closure and transport theory for high-collisionality electron–ion plasmas," Phys. Plasmas **20**, 042114 (2013).
[27] N. Krall and P. Liewer, "Low-frequency instabilities in magnetic pulses," Phys. Rev. A **4**, 2094 (1971).
[28] N. Gladd, "The lower hybrid drift instability and the modified two stream instability in high density theta pinch environments," Plasma Phys. **18**, 27 (1976).
[29] G. W. Hammett and F. W. Perkins, "Fluid moment models for Landau damping with application to the ion-temperature-gradient instability," Phys. Rev. Lett. **64**, 3019–3022 (1990).
[30] S. I. Braginskii, "Transport processes in a plasma," in *Reviews of Plasma Physics*, edited by M. A. Leontovich (Consultants Bureau, New York, 1965), Vol. 1, pp. 205–311.
[31] F. Trintchouk, M. Yamada, H. Ji, R. M. Kulsrud, and T. A. Carter, "Measurement of the transverse Spitzer resistivity during collisional magnetic reconnection," Phys. Plasmas **10**, 319–322 (2003).
[32] W. Fox, F. Sciortino, A. V. Stechow, J. Jara-Almonte, J. Yoo, H. Ji, and M. Yamada, "Experimental verification of the role of electron pressure in fast magnetic reconnection with a guide field," Phys. Rev. Lett. **118**, 125002 (2017).
[33] K. Tummel, L. Chen, Z. Wang, X. Y. Wang, and Y. Lin, "Gyrokinetic theory of electrostatic lower-hybrid drift instabilities in a current sheet with guide field," Phys. Plasmas **21**, 052104 (2014).
[34] J. Yoo, B. Na, J. Jara-Almonte, M. Yamada, H. Ji, V. Roytershteyn, M. R. Argall, W. Fox, and L.-J. Chen, "Electron heating and energy inventory during asymmetric reconnection in a laboratory plasma," J. Geophys. Res. **122**, 9264–9281, https://doi.org/10.1002/2017JA024152 (2017).
[35] Y. Hu, J. Yoo, H. Ji, A. Goodman, and X. Wu, "Probe measurements of electric field and electron density fluctuations at megahertz frequencies using in-shaft miniature circuits," Rev. Sci. Instrum. **92**, 033534 (2021).
[36] F. S. Mozer, M. Wilber, and J. F. Drake, "Wave associated anomalous drag during magnetic field reconnection," Phys. Plasmas **18**, 102902 (2011).
[37] J.-Y. Ji and E. D. Held, "Landau collision operators and general moment equations for an electron–ion plasma," Phys. Plasmas **15**, 102101 (2008).
[38] J. Yoo, Y. Hu, J. Y. Ji, H. Ji, M. Yamada, A. Goodman, K. Bergstedt, and A. Alt (2021). "Effects of coulomb collisions on lower hybrid drift waves inside a laboratory reconnection current sheet," DataSpace of Princeton University. https://dataspace.princeton.edu/handle/88435/dsp01x920g025r